IEEE Access
Multidisciplinary ⋮ Rapid Review ⋮ Open Access Journal

Received 15 June 2022, accepted 5 August 2022, date of publication 16 August 2022, date of current version 24 August 2022.

Digital Object Identifier 10.1109/ACCESS.2022.3199006

RESEARCH ARTICLE

On Mathematical Aspects of Evolution of Dislocation Density in Metallic Materials

NATALIA CZYŻEWSKA[1], JAN KUSIAK[2], PAWEŁ MORKISZ[1], PIOTR OPROCHA[1], MACIEJ PIETRZYK[2], PAWEŁ PRZYBYŁOWICZ[1], ŁUKASZ RAUCH[2], AND DANUTA SZELIGA[2]

[1]Faculty of Applied Mathematics, AGH University of Science and Technology, Kraków, Poland
[2]Faculty of Metals Engineering and Industrial Computer Science, AGH University of Science and Technology, Kraków, Poland

Corresponding author: Natalia Czyżewska (nczyzew@agh.edu.pl)

This work was supported by the National Science Centre (Narodowe Centrum Nauki—NCN), Poland, under Grant 2017/25/B/ST8/01823.

ABSTRACT This paper deals with the solution of delay differential equations describing evolution of dislocation density in metallic materials. Hardening, restoration, and recrystallization characterizing the evolution of dislocation populations provide the essential equation of the model. The last term transforms ordinary differential equation (ODE) into delay differential equation (DDE) with strong (in general, Hölder) nonlinearity. We prove upper error bounds for the explicit Euler method, under the assumption that the right-hand side function is Hölder continuous and monotone which allows us to compare accuracy of other numerical methods in our model (e.g. Runge-Kutta), in particular when explicit formulas for solutions are not known. Finally, we test the above results in simulations of real industrial process.

INDEX TERMS Delay differential equation, Euler method, metallic materials, Runge-Kutta method, strict error analysis.

I. INTRODUCTION

Numerous models of materials developed in the second half of the 20th century use external variables as independent ones [1]. The model output is a function of some process parameters (e.g., strain, temperature, strain rate), which are external variables and which are grouped in the vector p ($y = y(p)$, where y is the model output). The main drawback of this approach is that it does not properly take into account the history of the considered process. Namely, within these models once the conditions of the process change, the calculated material responses immediately by moving to a new equation of state and the model output is a function of new values of external variables. On the other hand, it was observed experimentally, see for example [2], that metallic materials in general show delay in the response to the change in processing conditions. Therefore, the rheological models, which include internal variables as independent parameters, were proposed in the literature. In the internal variable approach (IVM) the model output is a function of time t; again of some process parameters (e.g., temperature, strain rate), which we grouped in the vector p and internal variables, which we grouped in the vector q: (so now $y = y(t, p, q)$). Since the internal variables remember the state of the material, these models give more realistic description of materials behavior.

The model with one internal variable, which is the average dislocation density ρ, is usually considered for metallic materials. The model follows fundamental works of Kocks, Mecking, and Estrin [3], [4]. Main assumptions of this model are repeated briefly below. Since the stress during plastic deformation is governed by the evolution of dislocation populations, a competition of storage and annihilation of dislocations, which superimpose in an additive manner, controls a hardening. Thus, the flow stress σ_f accounting for softening is proportional to the square root of dislocation density

$$\sigma_f = a_7 + a_6 b\mu\sqrt{\rho}, \tag{1}$$

where a_6 is a material dependent coefficient, a_7 is stress due to lattice resistance or solution hardening, b is length of the Burgers vector, and μ is shear modulus (e.g. see [1, chapter 3.3]).

The associate editor coordinating the review of this manuscript and approving it for publication was Shuai Liu.

The evolution of dislocation populations is controlled by hardening ($d\rho/dt = A_1\dot{\varepsilon}$, where $\dot{\varepsilon}$ is the strain rate) and restoration ($\rho'(t) = -A_2(t)\rho(t)\dot{\varepsilon}(t)$) processes. During deformation the dislocation density increases in a monotonic way until the state of saturation is reached.

The Kocks-Mecking-Estrin (KEM) model has been intensively developed during last decades with the wide focus ranging from discrete dislocation dynamics [5] to phenomenological approaches [6]. Distinguishing between various types of dislocations (mobile, trapped) was an important objective of the research, see eg. recent publication [7]. A number of dislocation density reaction models were applied to describe the deformation of various superalloys, such as Ti-alloys [8], [9] and Ni-alloys [10]. Effect of reverse deformation on evolution of dislocations was investigated in [11]. Authors of [12] applied KEM based model to analyze fracture during deformation. Several researchers investigated deformation at lower temperatures, when recovery is a dominant softening mechanism [13]. However, at elevated temperatures an additional softening mechanism called recrystallization occurs. The term recrystallization is commonly used to describe the replacement of a deformation microstructure by new grains [14]. Processes of phase changes (transformations), which are common in metallic materials, compose nucleation and growth stages. It means that during this process the two phases can coexist. Recrystallization is classified as a specific type of the transformation, in which the part of the material with increased dislocation density due to deformation is considered an old phase and the part of the material with rebuilt microstructure and free of dislocations is considered a new phase. Two types of the recrystallization can be distinguished, dynamic which occurs during the deformation and static, which occurs after the deformation. The final microstructure and mechanical properties of the alloys are determined, to a large extent, by the recrystallization. The research on the recrystallization dates back to 19th century, and the fast development of the dynamic recrystallization theory was summarized in [14]. The most recent research on this process is described in [15]. A lot of factors have a significant effect on the recrystallization, including the stacking fault energy, the process conditions (temperature, strain rate), the grain size and few other metallurgical parameters. Modeling of recrystallization has been for decades based on the Johnson-Mehl-Avrami-Kolmogorov model, which is based on the external variables only and gives erroneous results when process conditions are changed. In the present work an approach based on the internal variable, which is a dislocation density, was proposed. Since various parts of the material during recrystallization can be in a different state and this process is launched when certain threshold of the accumulated energy is reached, the rate of this process depends on the history of the energy accumulation. The energy accumulated in the material in the form of dislocations from the past acts as the driving force for the current progress of the recrystallization. Similarly, the driving force during static recrystallization depends on the energy accumulated earlier in the material during deformation. This process is launched when certain threshold of the accumulated energy is reached and the rate of this process depends on the history of the energy accumulation. In the mathematical description of this phenomenon a delay differential equation (DDE) is a natural tool. This approach appeared first in [16]. For more details, see Chapter 3.3 in [1].

Accounting for the recrystallization in the KEM formalism is not so frequent and dedicated mainly to multiphase superalloys [17]. The focus is on physical background of the recrystallization in these alloys and there are no details of the numerical solution. To our knowledge, there are no publications connected with application of KEM model coupled with the recrystallization term to steels, which are still the most common constructional materials.

From the above reasoning, it turns out that the evolution of dislocation populations accounting for hardening, recovery, and recrystallization is given by

$$\rho'(t) = A_1(t)\cdot\dot{\varepsilon}(t) - A_2(t)\cdot\rho(t)\cdot\dot{\varepsilon}(t)^{1-a_9} - A_3(t)\cdot(\rho(t))^{a_8}\cdot\mathcal{R}(t-t_{cr}), \qquad t \geq 0, \tag{2}$$

where as before t is time, $\dot{\varepsilon}$ is the strain rate, A_1, A_2, A_3 are model parameters (sometimes time independent, but in most of real world cases dependent on other process parameters, such as t, $\dot{\varepsilon}$ etc.), and $a_8, a_9 \in [0, 1]$ are additional model coefficients. The function $\mathcal{R}$ is responsible for the delay in the response to the change in processing conditions, and in the most of practical considerations it is enough to consider

$$\mathcal{R}(s) = \mathbf{1}_{(0,+\infty)}(s)\cdot\rho(s). \tag{3}$$

In what follows, we will always use $\mathcal{R}$ in the form (3) in (2). In what follows, by a solution of (2) we mean any continuous function ρ, which we assume C^1 everywhere with the only possible exception at the point t_{cr}, where one-sided derivatives may disagree.

The rate of hardening is inversely proportional to the length of the Burgers vector b and the free path for dislocations l, that is $A_1 = 1/(bl)$ when $\dot{\varepsilon} > 0$ and $A_1 = 0$ when $\dot{\varepsilon} = 0$. The recovery and the recrystallization are temperature dependent processes following the Aarhenius law [18]. The average free path for dislocations l, the self-diffusion parameter A_2, and the grain boundary mobility A_3 in equation (2) are calculated as

$$l = \begin{cases} a_1 Z^{-a_{13}}, & \text{when } \dot{\varepsilon} > 0, \\ 0, & \text{when } \dot{\varepsilon} = 0, \end{cases} \tag{4}$$

$$A_2 = a_2 \exp\left(\frac{-a_3}{RT}\right), \tag{5}$$

$$A_3 = a_4 \frac{\mu b^2}{2D} \exp\left(\frac{-a_5}{RT}\right), \tag{6}$$

where: a_2 is self-diffusion coefficient, a_3 is activation energy for self-diffusion, a_4 is coefficient of the grain boundary mobility, a_5 is activation energy for grain boundary mobility, D is austenite grain size, $Z = \dot{\varepsilon}\exp(Q/(RT))$, is the Zener-Hollomon parameter, Q is activation energy for deformation, R is the universal gas constant equal to 8.314 J/mol,

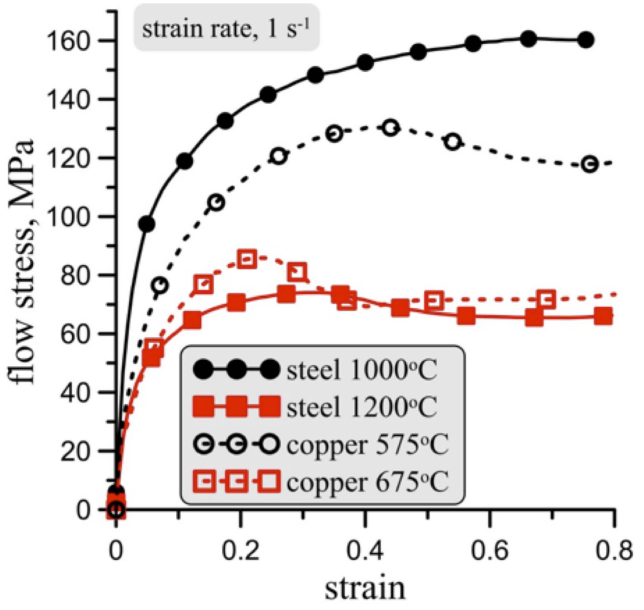

FIGURE 1. Typical responses of metallic materials subjected to deformation at elevated temperatures, results of the tests for DP steel [19] and copper [20].

and a_1, a_{13} are auxiliary model coefficients. Note that in real industrial process even T varies in time, so coefficients A_1, A_2, A_3 are complicated functions changing in time.

Critical dislocation density for recrystallization is calculated as

$$\rho_{cr} = a_{11} + a_{12} Z^{a_{10}} \tag{7}$$

where a_{10}, a_{11}, a_{12} are coefficients, and t_{cr} is the time between beginning of deformation and beginning of recrystallization (i.e. the moment of reaching ρ_{cr}). Note that ρ_{cr} depends on Z which also changes in time. In simplified approach, ρ_{cr} will be constant, but in practice it is not. In any case, we are interested in the first time that this value is reached (curves representing ρ and ρ_{cr} intersect), which is by the definition value of t_{cr}.

In real world, measurement of dislocation density during the process is difficult. Fortunately, flow stress can be measured, and it is dependent on the dislocation density, which evolution is given by equation (2). Measurements of flow stress from experiments for different materials are presented in Fig. 1.

Besides numerical simulations, we will perform a detailed theoretical analysis of (2), and there are a few good reasons to do that. First of all, it is hard to find in the literature mathematical tools that can be directly applied to this type of equations, while in recent years some studies of its numerical evolution were undertaken. Classical literature for ordinary differential equations (ODE), e.g. [21], [22], assumes some regularity of right-hand side function, commonly Lipschitz condition. Similar assumptions occur for delay differential equations, cf. [23], [24]. Unfortunately, there is no strict mathematical analysis of the error even in the case of standard numerical methods like explicit Euler method, for considered here nonlinear delay differential equations with a locally Hölder continuous and monotone right-hand side function. In the recent literature weakened conditions appear with regards to stochastic delay differential equations (e.g. [25], [26]), stochastic functional differential equations with infinite delay [27], uncertain delay differential equations driven by a canonical Liu process [28], neutral fractional order time delay systems [29] or in differential equations with time-dependent delay (c.f. [30] where only stability of equilibria were studied).

In our opinion it is valuable to show that results of these simulations reflect the real behavior of the system. Fortunately, analytic solutions and rigorous formulas can be used for numerical tests on this equation for simplified equations derived from (2), especially the cases when coefficients A_i are no longer time (or other process parameters) dependent. As a result of this study we want to ensure that numerical methods, which are accurate at one hand, and have low computational cost at the same time. As we will see, there are good candidates here (as we prove they behave well for simplified models).

While nowadays there is high popularity in methods of higher order (e.g. Runge-Kutta scheme), they are not suitable for our needs. First of all, observe that in (2) the right-hand side function is only monotone and locally Hölder continuous, however it is not differentiable at 0 and it is not even globally Lipschitz continuous (recall that the global Lipschitz condition is usually imposed in the literature). Yet another problem in the case of delayed equations, is that in practice in the case of higher order we will need value of delayed function in points not used in mesh of computation. This leads to interpolation of these values, possibly canceling effect of higher order, and making precise error analysis extremely problematic. Taking all the above reasons into account, we decided to stick with classical Euler scheme whose correctness and suitability we are convinced both numerically and mathematically. In particular, we provide in Theorem 3.2 the error bounds for the classical Euler scheme under such irregular assumptions. Moreover, numerical results reported in Section IV confirmed its good behavior, when applied to the equation (2) with real-world parameters. For further numerical experiments in real-world setting we refer the reader to our recent paper [31].

The paper is organized as follows. Section II is devoted to existence and uniqueness of solutions of (2). Section III contains error behavior analysis for explicit Euler method with some discussion why we finally chose it for our main numerical experiments. Finally, in Section IV some numerical results are given, with simulations for (2) with real world parameters of selected metallic materials (copper and Dual Phase steel, DP steel for short) at the end.

II. EXISTENCE AND UNIQUENESS OF SOLUTIONS OF SOME INSTANCES OF (2)

In this section we will consider (2) with some relatively mild additional conditions on time-dependent coefficients

A_1, A_2, A_3 and $\dot{\varepsilon}$ (mainly that they are bounded, end extremal values satisfy some relations bonding them together). Before we can prove main results of this section, we will consider the following auxiliary delay differential equation obtained by simplification of (2) to the form

$$\rho'(t) = A_1 - A_2 \cdot \rho(t) - A_3 \cdot (\rho(t))^{a_8} \cdot \mathbf{1}_{(t_{cr},+\infty)}(t) \cdot \rho(t - t_{cr}), \tag{8}$$

where $a_8 \in [0, 1]$ and $A_1, A_2, A_3 > 0$ are constant. Observe that in (8), compared to (2), we assume constant strain rate $\dot{\varepsilon}(t) \equiv 1$, and by convention function $\mathcal{R}$ is given by (3). Properties of this simplified equation will allow us to approximate evolution of (2).

A. EXISTENCE AND UNIQUENESS OF SOLUTION

We start with presenting two auxiliary results on (8), which will help us to analyze (2). Note that the case $a_8 = 0$ is very similar to the simple delayed equation $\rho'(t) = A_1 - A_2 \cdot \rho(t) - A_3 \cdot \rho(t - \tau)$ considered in [32]. Unfortunately, we may not use directly formulas of solutions from there, since in our case of (8), influence of delayed term is also delayed by characteristic function in (3). In [32] it was pointed out that too large value of τ with respect to A, B, C can result in unbounded oscillations and as a result negative values of ρ. In what follows we will see that the condition $\frac{A_3}{A_2} < 1$ always prevents it, while as reported in [32], cases $\frac{A_3}{A_2} \geq 1$ may lead to unstable solutions. The situation in this case is much dependent on the value of ρ_{cr}, however. The analysis of (8) will lead to analogous conditions on coefficients in (2). However as we will see later, our model (with real world parameters) will satisfy these assumptions. The following result is an adaptation of the proof of Theorem 3.2. in [24] to delay differential equations (8). The argument is standard, however, we present it for the reader's convenience.

Lemma 2.1: Let $\rho\colon [0, \sigma) \to \mathbb{R}$ *be a noncontinuable solutions of delay differential equations* (8) *and assume that* $\sigma < +\infty$. *Then* $\lim_{t\to\sigma^-} |\rho(t)| = +\infty$.

Proof: There is $j \geq 0$ such that $jt_{cr} < \sigma \leq (j+1)t_{cr}$. But then we can view ρ as a noncontinuable solution of the ODE defined for $0 \leq t < \sigma + t_{cr}$:

$$x'(t) = A_1(t) \cdot \dot{\varepsilon}(t) - A_2(t) \cdot x(t) \cdot \dot{\varepsilon}(t)^{1-a_9} - A_3(t) \cdot (x(t))^{a_8} \cdot \mathbf{1}_{(0,+\infty)}(t) \cdot \rho(t - t_{cr}).$$

If ρ was bounded, then by standard argument for ODEs (e.g. see [33, Theorem 2.1]) ρ can be continued beyond σ which is a contradiction. □

Lemma 2.2: Assume that $\frac{A_3}{A_2} < 1$ *and* $a_8 = 0$. *The solutions of delay differential equations* (8) *with the initial-value condition*

$$0 \leq \rho(0) = \rho_0 < \rho_{cr} < A_1/A_2; \quad \rho(t) = \rho_0 \text{ for } t < 0$$

exist for any $t \geq 0$ *and are bounded by* $[0, A_1/A_2]$.

Proof: It is easy to verify that for $t \leq t_{cr}$ the solution $\rho(t)$ exists, is increasing and contained in the interval $(0, \rho_{cr})$. After reaching $t = t_{cr}$, discontinuity in the vector field disappears, and (8) becomes standard delay differential equation with continuous initial condition, defined by solution of (8) on the interval $[0, t_{cr}]$

$$\rho'(t) = A_1 - A_2\rho(t) - A_3\rho(t - t_{cr}).$$

In the case that there is a solution that cannot be continued on $\mathbb{R}_+$ it must leave the interval $[0, A_1/A_2]$ first, see Lemma 2.1. Denote

$$\gamma = \sup\{t : \rho(s) \in [0, A_1/A_2] \text{ for all } 0 \leq s \leq t\}$$

and assume that $\gamma < \infty$. It is clear that $\gamma > 0$ and there is a decreasing sequence t_n, such that $\lim_{n\to\infty} t_n = \gamma$, $\rho(t_n)$ is well defined (i.e. t_n is in domain of ρ) and $\rho(t_n) \notin [0, A_1/A_2]$.

By definition $\rho(\gamma) \in \{0, A_1/A_2\}$. Let us consider two cases.

1) Assume first that $\rho(\gamma) = A_1/A_2$. If $\rho(\gamma - t_{cr}) > 0$ then $\rho'(t) < 0$ for $t \in (\gamma - \delta, \gamma + \delta)$ for sufficiently small δ which is impossible, because for small δ, $\rho'(t)$ is continuous on $(\gamma, \gamma + \delta)$ contradicting the choice of sequence t_n.
   Let us assume now that $\rho(\gamma - t_{cr}) = 0$. This implies that there exists $\delta > 0$ such that for $t \in (\gamma - \delta, \gamma + \delta)$ function r defined by $r(t) = A_1/A_2$ for $t \in [\gamma, \gamma + \delta)$ and $r(t) = \rho(t)$ for $t < \gamma$ is continuous. But then, the function $x(t) = \rho(t) - r(t)$ is a solution of the ODE with continuous vector field defined by $x'(t) = -A_2x(t)$ for $t \in (\gamma - \delta, \gamma]$ and $x'(t) = -A_2x(t) - A_3\rho(t - t_{cr})$ for $t \in (\gamma, \gamma + \delta)$, with initial condition $x(\gamma) = 0$. It is clear that x as a solution of that equation must satisfy $x(t) \leq 0$ because for $x > 0$ the vector field is negative. Therefore, for $t \in (\gamma, \gamma + \delta)$ we have $\rho(t) \leq \frac{A_1}{A_2} \leq \rho(\gamma)$. This is in contradiction with the choice of sequence t_n.
2) Assume next that $\rho(\gamma) = 0$. There is δ such that for $t \in (\gamma - \delta, \gamma + \delta)$ we have $\frac{A_3}{A_2} + \frac{A_2}{A_1}|\rho(t)| < 1$. But then, for all these t we have a lower bound for the values of the vector field

$$\rho'(t) \geq A_1 - |\rho(t)|A_2 - A_3\frac{A_1}{A_2} \geq A_1\left(1 - \frac{A_2}{A_1}|\rho(t)| - \frac{A_3}{A_2}\right) > 0$$

   showing that ρ is an increasing function on the interval $(\gamma - \delta, \gamma + \delta)$. A contradiction again.

Indeed, the solution of (8) is bounded and contained in $[0, A_1/A_2]$, which then implies that it can also be continued onto $\mathbb{R}_+$, see Lemma 2.1. □

While we state the following result for $a_8 > 0$ in practice we will be interested only in $a_8 \in [0, 1]$. The proof is standard, we leave details to the reader.

Lemma 2.3: Assume that $\frac{A_3}{A_2} < 1$ *and* $a_8 > 0$. *The solutions of delay differential equations* (8) *and with initial-value condition*

$$0 \leq \rho(0) = \rho_0 < \rho_{cr} < A_1/A_2; \quad \rho(t) = \rho_0 \text{ for } t < 0$$

exist for any $t \geq 0$ *and are bounded by* $[0, A_1/A_2]$.

Remark 2.4: In the following theorem we may replace $m\alpha_2$ *by* $\inf \dot{\varepsilon} A_2$ *and* $M\beta_1$ *by* $\sup \dot{\varepsilon} A_1$. *This way it can be applied to a slightly larger class of equations.*

Remark 2.5: In practice, the value of temperature $T(t)$ *is much higher than* 0 *and by physical constraints also bounded from the above. So if* $\dot{\varepsilon}(t) > m > 0$ *then* $Z(t) \subset [a, b] \subset (0, +\infty)$ *and as a consequence all the coefficients* $A_i(t)$ *are bounded and separated from zero.*

Theorem 2.6: Assume that there are positive constants $0 < \alpha_i \leq \beta_i$ *and* $0 < m \leq M$ *such that coefficients* $A_i(t) \in [\alpha_i, \beta_i]$ *(for each* $t \geq 0$*; this takes into account other process parameters that these coefficients are dependent) and* $\dot{\varepsilon}(t) \in [m, M]$ *for every* $t \geq 0$. *Additionally assume that* $\frac{\alpha_3}{m\alpha_2} < 1$ *and either* $a_8 > 0$ *or* $\frac{\beta_3}{m\beta_2} < 1$. *Then the solutions of delay differential equations* (2) *with the initial-value condition*

$$0 \leq \rho(0) = \rho_0 < \rho_{cr} < \frac{M\beta_1}{m\alpha_2}; \quad \rho(t) = \rho_0 \text{ for } t < 0$$

exist for any $t \geq 0$ *and are bounded by* $[0, \frac{M\beta_1}{m\alpha_2}]$ *and are unique.*

Proof: Consider the following equations with constant coefficients:

$$z'(t) = M\beta_1 - m\alpha_2 z(t) - \alpha_3 \mathbf{1}_{[t_{cr},\infty)}(t) z(t - t_{cr}) \tag{9}$$

and with initial-value condition $z(t) = \rho_0$ for all $t \leq 0$ and

$$w'(t) = m\alpha_1 - M^{1-a_9}\beta_2 w(t) - \beta_3 \mathbf{1}_{[t_{cr},\infty)}(t) w(t - t_{cr}) \tag{10}$$

and with initial-value condition $w(t) = 0$ for all $t \leq 0$ where t_{cr} is provided solution of (2), provided it exists. In the other case we omit delay term in (9) and (10). By Lemmas 2.2 and 2.3 solutions of (9) and (10) exist for every $t > 0$ and $z(t) < \frac{M\beta_1}{m\alpha_2}$ while $w(t) \geq 0$. In fact, $w(t) \geq 0$ when $a_8 > 0$ despite of relations between other coefficients. Simple calculations yield that for $t < t_{cr}$ we have $z'(t) - \rho'(t) \leq 0$ and $\rho'(t) - w'(t) \geq 0$ which implies that $\rho(t)$ exists for $t \in [0, t_{cr}]$ and $w(t) \leq \rho(t) \leq z(t)$ and this inequality can be recursively extended onto further intervals $[nt_{cr}, (n+1)t_{cr}]$ which completes the proof of boundedness of solutions.

Consider time interval $[nt_{cr}, (n+1)t_{cr})$ for $n = 0, 1, \ldots$. We may view (11) on each of these intervals as ODE. Let

$$f(t, x) = A_1(t) \cdot \dot{\varepsilon}(t) - A_2(t) \cdot x \cdot \dot{\varepsilon}(t)^{1-a_9} - A_3(t) \cdot x^{a_8} \cdot \mathcal{R}(t - t_{cr})$$

where on each of the above intervals delay term $\mathcal{R}(t - t_{cr})$ can be regarded as a function of t but independent of solution. In fact we can view $\mathcal{R}(t - t_{cr})$ as a function defined for all $t \in \mathbb{R}$ by putting $\mathcal{R}(t - t_{cr}) = \mathcal{R}(nt_{cr})$ for all $t > (n+1)t_{cr}$. This way we may regard (2) as associated ODE

$$\rho'(t) = f(t, \rho(t)) \tag{11}$$

with initial condition $\rho(nt_{cr}) := \lim_{s \to nt_{cr}^-} \rho(s)$, since values $\rho(s)$ for $s \in [(n-1)t_{cr}, nt_{cr})$ have already been determined. It is obvious that $\rho(t_{cr}) \geq 0$. Note that there are $\delta, \alpha > 0$ such that for $x \in [0, \delta]$ we have $f(t, x) > \alpha$, so in particular $\rho(t)$ is bounded away from 0, provided it is defined. We already know that there is a solution ρ of (2) (so also (11)) in $[nt_{cr}, (n+1)t_{cr})$ and assume that $\bar{\rho}$ is another solution in $[t_{cr}, 2t_{cr})$, but with the same initial value as ρ, i.e., $\bar{\rho}(t_{cr}) = \rho(t_{cr})$. Then we have

$$\frac{d}{dt}(\rho(t) - \bar{\rho}(t))^2 = 2(\rho(t) - \bar{\rho}(t))(f(t, \rho(t)) - f(t, \bar{\rho}(t))) \leq 0, \tag{12}$$

since for all t the function $(0, +\infty) \ni x \mapsto f(t, x)$ is nonincreasing (recall $\rho(t) \geq 0$ for all $t \geq 0$), hence

$$0 \leq (\rho(t) - \bar{\rho}(t))^2 \leq (\rho(nt_{cr}) - \bar{\rho}(nt_{cr}))^2 = 0. \tag{13}$$

Repeating the above arguments inductively on consecutive intervals $[nt_{cr}, (n+1)t_{cr})$ we complete the proof. □

Remark 2.7: In practical applications, the condition $\dot{\varepsilon}(t) \geq m > 0$ *will not be usually satisfied. The reason is that inside the metallic material usually it will take some time to observe* $\dot{\varepsilon}(t) > 0$. *However after some time, say* T_0 *we will have* $\dot{\varepsilon}(t) > m$ *for all* $t > T_0$ *and at the same time* ρ *will not diverge too much from* ρ_0. *The reader may check that in these cases, statements of Theorem 2.6 are still valid.*

The same reasoning can be applied to other coefficients.

B. SOME SOLUTIONS OF THE TOY MODEL (8) AND EXISTENCE OF t_{cr}

For the equation (8) we can give explicit formula for solution in the case when $a_8 \in \{0, 1\}$. For the fractional values of a_8 it is rather hard to provide analytic formulas. On the other hand, we may view the above two cases of a_8 as bounds for intermediate values. The main utility of these formulas, is that they can be used to strict control of error in preliminary numerical experiments. As usual, let us assume that

$$0 \leq \rho_0 < \rho_{cr} < A_1/A_2. \tag{14}$$

Under the assumption above the solution ρ attains the critical value ρ_{cr} in finite time t_{cr}, and it is not hard to check that

$$t_{cr} = \frac{1}{A_2} \ln\Big(\frac{\rho_0 - (A_1/A_2)}{\rho_{cr} - (A_1/A_2)}\Big). \tag{15}$$

Namely, for $t \in [0, t_{cr}]$ the equation (8) is reduced to a simple linear equation with the solution

$$\rho(t) = \frac{A_1}{A_2} + \Big(\rho_0 - \frac{A_1}{A_2}\Big)e^{-A_2 t}, \tag{16}$$

which is a strictly increasing function and $\rho(t_{cr}) = \rho_{cr}$. In the intervals $[nt_{cr}, (n+1)t_{cr}]$, $n \in \mathbb{N}$, we solve the equation (8) recursively as follows. Let us denote by ϕ_{n-1} the solution ρ in the interval $t \in [(n-1)t_{cr}, nt_{cr}]$ (ϕ_0 in $[0, t_{cr}]$ is given by (16)). We have two cases:

(i) $\mathbf{a_8 = 0}$: The solution with the initial value $\rho(nt_{cr}) = \phi_{n-1}(nt_{cr})$ is

$$\rho(t) = e^{-A_2(t - nt_{cr})} \cdot \Big(\phi_{n-1}(nt_{cr}) + \int_{nt_{cr}}^{t} e^{A_2(s - nt_{cr})} \cdot \Big(A_1 - A_3 \cdot \phi_{n-1}(s - t_{cr})\Big) ds\Big), \tag{17}$$

for $t \in [nt_{cr}, (n+1)t_{cr}]$.

(ii) $\mathbf{a_8 = 1}$: The initial value $\rho(nt_{cr}) = \phi_{n-1}(nt_{cr})$ leads to the solution

$$\rho(t) = e^{-\int_{nt_{cr}}^{t} p_{n-1}(s)ds} \cdot \left(\phi_{n-1}(nt_{cr}) + A_1 \cdot \int_{nt_{cr}}^{t} e^{\int_{nt_{cr}}^{s} p_{n-1}(u)du} ds\right), \tag{18}$$

where

$$p_{n-1}(t) = A_2 + A_3 \cdot \phi_{n-1}(t - t_{cr}), \quad t \in [nt_{cr}, (n+1)t_{cr}]. \tag{19}$$

Note that both solutions are given in integral form, which most likely is impossible to present as explicit functions in the case $a_8 = 1$, since we have doubly exponential terms under integral. For the case $a_8 = 0$ it seems possible to provide some formulas (similarly to [32]), however their complexity increases rapidly with multiplies of t_{cr}, mainly because vector field is discontinuous.

On the other hand, equations (17) and (18) can be treated with numerical integration with rigorous control of numerical errors. This way we can accurately estimate numerical errors of numerical solutions of these equations (e.g. by explicit Euler method). This gives us a chance for rigorous comparison of various numerical methods for solving equations of type (8), possibly ensuring similar behavior of numerical approximations of its further generalizations.

Remark 2.8: The assumption that $A_1 > 0$ seems to be crucial in order to have a nontrivial problem, since, in the case when $A_1 = 0$, we get by (14) that $\rho_0 = \rho_{cr} = 0$ and $t_{cr} = 0$. Moreover, the equation (8) becomes the following Bernoulli equation

$$\rho'(t) = -A_2 \cdot \rho(t) - A_3 \cdot (\rho(t))^{a_8+1}, \quad t > 0, \tag{20}$$

which, under the initial value $\rho_0 = 0$, has the following trivial solution $\rho(t) = 0$ for all $t \in [0, +\infty)$ and all $a_8 \in [0, 1]$. By Theorem 2.3 all solutions of (8) tend to the zero solution when $A_1 \to 0+$. Hence, only the case when $A_1 > 0$ is of practical interest. It is worth mentioning, that it is always the case in considered models.

Unfortunately in applications we cannot assume that coefficients A_i are time independent. Then the question arise to which extent the new equation is similar. The first step will be to show that critical time t_{cr}, under certain assumptions on A_1, A_2, always exists also in that case. Assume that assumptions of Theorem 2.6 are satisfied, in particular coefficients A_i as well as $\dot{\varepsilon}$ are bounded, i.e. $A_i(t) \in [\alpha_i, \beta_i]$ and $\dot{\varepsilon}(t) \in [m, M]$ for every $t \geq 0$.

Consider time-dependent version of (8) before reaching t_{cr} derived from (2) with "smallest possible" vector fiels, that is the equation (stated for $t \geq 0$)

$$\rho'(t) = mA_1(t) - M^{1-a_9}A_2(t) \cdot \rho(t), \quad \rho(0) = \rho_0 \geq 0. \tag{21}$$

Hence

$$\rho(t) = e^{-M^{1-a_9}\int_0^t A_2(s)ds} \cdot \left(\rho_0 + m\int_0^t e^{M^{1-a_9}\int_0^s A_2(u)du} A_1(s)ds\right), \tag{22}$$

which is clearly continuous and positive function on $[0, +\infty)$, and since both A_1, A_2 are bounded away from zero, we also have

$$\lim_{t\to+\infty} e^{\int_0^t A_2(s)ds} = +\infty,$$
$$\lim_{t\to+\infty} \int_0^t e^{\int_0^s A_2(u)du} A_1(s)ds = +\infty. \tag{23}$$

Therefore solution of both (22) and (2) satisfy

$$\limsup_{t\to+\infty} \rho(t) \geq \frac{m}{M^{1-a_9}} \limsup_{t\to+\infty} \frac{A_1(t)}{A_2(t)}.$$

In particular, when $\limsup_{t\to+\infty} \frac{A_1(t)}{A_2(t)} > \frac{M^{1-a_9}\rho_{cr}}{m}$ then there exists $t_{cr} > 0$ such that the solution ρ of (21) satisfies $\rho(t_{cr}) = \rho_{cr}$ (and by continuity we may assume that t_{cr} is smallest among all such times).

For example, let us consider the equation (2) with $a_9 = 0$, time independent but positive A_1, A_2, continuous $\dot{\varepsilon}$ and, as before, assume that $\dot{\varepsilon}(t) \geq m > 0$ for all $t \geq 0$. Hence, we are considering time-dependent version of (8), with $A_1(t) = A_1\dot{\varepsilon}(t)$, $A_2(t) = A_2\dot{\varepsilon}(t)$ and $A_3(t) = A_3$. Under the assumption (14) we have, by the above considerations, that there always exists $t_{cr} > 0$, since in that case $\limsup_{t\to+\infty} \rho(t) = A_1/A_2 > \rho_{cr}$. Moreover, it can be shown that

$$t_{cr} = \varepsilon^{-1}\left(\frac{1}{A_2}\ln\left(\frac{\rho_0 - (A_1/A_2)}{\rho_{cr} - (A_1/A_2)}\right) + \varepsilon(0)\right), \tag{24}$$

where ε^{-1} is the inverse function for ε, which exists since ε is strictly increasing. Note that in the case when $\dot{\varepsilon} \equiv 1$ we restore from (24) the equation (15). Nevertheless, only in this particular case we know the closed formula for t_{cr}. In general the nonlinear equation $\rho(t_{cr}) = \rho_{cr}$ has to be solved numerically.

As long as t_{cr} is calculated, we can repeat arguments presented earlier in Section II-B and provide formulas for solutions when $a_8 \in \{0, 1\}$. As before, for $t \in [nt_{cr}, (n+1)t_{cr}]$, $n \in \mathbb{N}$, we solve the equation (8) with time-dependent A_1, A_2, A_3 recursively. Let us denote by ϕ_{n-1} the solution ρ in the interval $t \in [(n-1)t_{cr}, nt_{cr}]$, where ϕ_0 in $[0, t_{cr}]$ is given by

$$\phi_0(t) = e^{-\int_0^t A_2(s)ds} \cdot \left(\rho_0 + \int_0^t e^{\int_0^s A_2(u)du} A_1(s)ds\right). \tag{25}$$

We consider the following two cases:

(i) $\mathbf{a_8 = 0}$: Then for $t \in [nt_{cr}, (n+1)t_{cr}]$, $n \in \mathbb{N}$, the solution is given by

$$\rho(t) = e^{-\int_{nt_{cr}}^{t} A_2(s)ds} \cdot \left(\phi_{n-1}(nt_{cr}) + \int_{nt_{cr}}^{t} e^{\int_{nt_{cr}}^{s} A_2(u)du} \cdot q_{n-1}(s)ds\right), \tag{26}$$

where

$$q_{n-1}(t) = A_1(t) - A_3(t) \cdot \phi_{n-1}(t - t_{cr}). \tag{27}$$

(ii) $\mathbf{a_8 = 1}$: Then for $t \in [nt_{cr}, (n+1)t_{cr}]$, $n \in \mathbb{N}$, the solution is

$$\rho(t) = e^{-\int_{nt_{cr}}^{t} p_{n-1}(s)ds} \cdot \left(\phi_{n-1}(nt_{cr}) + \int_{nt_{cr}}^{t} e^{\int_{nt_{cr}}^{s} p_{n-1}(u)du} \cdot A_1(s)ds\right), \tag{28}$$

where

$$p_{n-1}(t) = A_2(t) + A_3(t) \cdot \phi_{n-1}(t - t_{cr}), \quad t \in [nt_{cr}, (n+1)t_{cr}]. \tag{29}$$

Despite, the formulas being slightly more complicated, they can be effectively used within the process of evaluation of accuracy and correctness of numerical methods used to solve time-dependent versions of (8).

III. ERROR ANALYSIS OF THE EXPLICIT EULER METHOD

Since in the case when $a_8 \in (0, 1)$ the exact formulas for the solution of (2) are not known, we use the suitable numerical methods to approximate ρ on a finite time interval. We are interested in the error analysis for solutions of (2) after reaching t_{cr}, since delay activates at this point. This approach will allow us to impose some reasonable assumptions on continuity of vector field. It will be visible in assumptions (F1)-(F4) below; see also Remark 3.7.

We consider the (general) delay differential equation

$$z'(t) = f(t, z(t), z(t - t_{cr})), \quad t \geq 0, \tag{30}$$

with a given right-hand side function $f : [0, +\infty) \times \mathbb{R} \times \mathbb{R} \to \mathbb{R}$ and where $z(t) = \eta \in \mathbb{R}$ for $t \in [-t_{cr}, 0]$.

For fixed $n \in \mathbb{N}$ the *explicit Euler method* that approximates a solution $z = z(t)$ of (30) for $t \in [0, (n+1)t_{cr}]$ is defined recursively for subsequent intervals. Namely, let $N \in \mathbb{N}$ and

$$t_k^j = jt_{cr} + kh, \quad k = 0, 1, \ldots, N, \ j = 0, 1, \ldots, n,$$

where

$$h = \frac{t_{cr}}{N}. \tag{31}$$

Note that $\{t_k^j\}_{k=0}^N$ is uniform discretization of the subinterval $[jt_{cr}, (j+1)t_{cr}]$. Discrete approximation of z in $[0, t_{cr}]$ is defined by

$$y_0^0 = \eta, \tag{32}$$

$$y_{k+1}^0 = y_k^0 + h \cdot f(t_k^0, y_k^0, \eta), \quad k = 0, 1, \ldots, N-1. \tag{33}$$

Let us assume that the approximations $y_k^{j-1} \approx z(t_k^{j-1})$, $k = 0, 1, \ldots, N$, have already been defined in the interval $[(j-1)t_{cr}, jt_{cr}]$ (for $j = 1$ it was done in (32) and (33)). Then for $j = 1, 2, \ldots, n$ we take

$$y_0^j = y_N^{j-1}, \tag{34}$$

$$y_{k+1}^j = y_k^j + h \cdot f(t_k^j, y_k^j, y_k^{j-1}), \quad k = 0, 1, \ldots, N-1, \tag{35}$$

as the approximation of z in $[jt_{cr}, (j+1)t_{cr}]$.

In this section we present rigorous analysis of the error of the explicit Euler method under the nonstandard assumptions on the right-hand side function f of the equation (30). Namely, we assume that f is monotone and locally Hölder continuous instead of the global Lipschitz continuity. According to the authors knowledge, there is lack of such analysis in the literature (cf. [21], [22], [23]), since we consider a non-Lipschitz case. It should be mentioned that in case of numerical integration methods really strict error analysis is complicated, otherwise any method can be improved using the knowledge of its error behavior. Strict truncation error evaluation is an elusive goal of scholars in numerical integration.

Let us emphasize once again, that we cannot apply higher order methods under out assumptions (such us Runge-Kutta schemes), since we do not assume that function f is differentiable. Observe that indeed it is the case of our main equation (2), since the right-hand side function of (2) is not differentiable at 0 when $a_8 \in (0, 1)$.

For the right-hand side function $f : [0, +\infty) \times \mathbb{R} \times \mathbb{R} \to \mathbb{R}$ in the equation (30) we impose the following assumptions:

(F1) $f \in C([0, +\infty) \times \mathbb{R} \times \mathbb{R}; \mathbb{R})$.

(F2) There exists a constant $K \geq 0$ such that for all $(t, y, z) \in [0, +\infty) \times \mathbb{R} \times \mathbb{R}$

$$|f(t, y, z)| \leq K(1 + |y|)(1 + |z|).$$

(F3) For all $(t, z) \in [0, +\infty) \times \mathbb{R}$, $y_1, y_2 \in \mathbb{R}$

$$(y_1 - y_2)(f(t, y_1, z) - f(t, y_2, z)) \leq 0.$$

(F4) There exist $L \geq 0$, $\alpha, \beta, \gamma \in (0, 1]$ such that for all $t_1, t_2 \in [0, +\infty)$, $y_1, y_2, z_1, z_2 \in \mathbb{R}$

$$\begin{aligned} |f(t_1, y_1, z_1) - f(t_2, y_2, z_2)| \leq L\Big(&(1 + |y_1| + |y_2|) \cdot (1 + |z_1| + |z_2|) \cdot |t_1 - t_2|^{\alpha} \\ &+ |y_1 - y_2|^{\beta} \\ &+ (1 + |z_1| + |z_2|)|y_1 - y_2|^{\gamma} \\ &+ (1 + |y_1| + |y_2|)|z_1 - z_2|\Big). \end{aligned}$$

In the following fact we provide an example of the right-hand side function that satisfies the assumptions (F1)-(F4). In what follows we use this function in order to approximate the solution of (2) in the case when $a_8 \in (0, 1)$, see also Remark 3.7. The proof of this fact is standard and we leave it to the reader.

Lemma 3.1: Let the functions $A, B, C : [0, +\infty) \to [0, +\infty)$ *satisfy Hölder condition with the Hölder exponent* $\alpha \in (0, 1]$ *and with the Hölder constant* $H \in [0, +\infty)$, $\varrho \in (0, 1]$ *and define a function* $\tilde{f} : [0, +\infty) \times \mathbb{R} \times \mathbb{R} \to \mathbb{R}$ *as follows*[1]

$$\tilde{f}(t, y, z) = A(t) - B(t) \cdot sgn(y) \cdot |y| - C(t) \cdot sgn(y) \cdot |y|^{\varrho} \cdot |z|. \tag{36}$$

If the functions A, B, C *are bounded in* $[0, +\infty)$, *then the function* $\tilde{f}$ *satisfies (F1)-(F4) with* $K = \|A\|_\infty + \|B\|_\infty + \|C\|_\infty$, $L = \max\{3H, \|B\|_\infty, 2\|C\|_\infty\}$, $\alpha = \alpha$, $\beta = 1$ *and* $\gamma = \varrho$.

The following theorem is the main result of this section. It states the upper bound on th error of the Euler algorithm under the mild assumptions (F1)-(F4). We want to underline here that up to our knowledge there are no such results in the literature, since in standard situation at least the global Lipschitz condition is satisfied. Unfortunately, due to the form of the main equation (2), this condition is not satisfied, which supports necessity of the following result.

Theorem 3.2: Let $\eta \in \mathbb{R}$ *and let* f *satisfy (F1)-(F4). Fix* $n \in \mathbb{N}$. *Then there exist* $C_0, C_1, \ldots, C_n \geq 0$ *such that for sufficiently large* $N \in \mathbb{N}$ *the following holds*

$$\max_{0 \leq k \leq N} |\phi_0(t_k^0) - y_k^0| \leq C_0(h^\alpha + h^\beta + h^\gamma), \tag{37}$$

and for $j = 1, 2, \ldots, n$

$$\max_{0 \leq k \leq N} |\phi_j(t_k^j) - y_k^j| \leq C_j(h^{1/2} + h^\alpha + h^\beta + h^\gamma), \tag{38}$$

where $\phi_j = \phi_j(t)$ *is the solution of (30) on the interval* $[jt_{cr}, (j+1)t_{cr}]$ *and sequences* y_k^j, t_k^j *are calculated using explicit Euler method as described in* (34).

We want to underline here that the theorem above gives the error estimates for the Euler scheme on the fixed and bounded time horizon $[0, (n+1)t_{cr}]$. This is crucial, since the discretization parameter N depends on n.

In order to prove Theorem 3.2 we need several auxiliary lemmas. Note that the same symbol may be used for different constants.

Lemma 3.3: Let us consider the following ordinary differential equation

$$z'(t) = g(t, z(t)), \quad t \in [a, b], \quad z(a) = \eta, \tag{39}$$

where $-\infty < a < b < +\infty$, $\eta \in \mathbb{R}$ *and* $g : [a, b] \times \mathbb{R} \to \mathbb{R}$ *satisfies the following conditions*:

(G1) $g \in C([a, b] \times \mathbb{R}; \mathbb{R})$.

(G2) *There exists* $K > 0$ *such that for all* $(t, y) \in [a, b] \times \mathbb{R}$

$$|g(t, y)| \leq K(1 + |y|).$$

(G3) *For all* $t \in [a, b]$, $y_1, y_2 \in \mathbb{R}$

$$(y_1 - y_2)(g(t, y_1) - g(t, y_2)) \leq 0.$$

Then the equation (39) *has a unique* C^1 *solution in* $[a, b]$,

$$\sup_{t \in [a,b]} |z(t)| \leq (|\eta| + K(b-a))e^{K(b-a)}, \tag{40}$$

and for all $t, s \in [a, b]$

$$|z(t) - z(s)| \leq \bar{K}|t - s|, \tag{41}$$

where $\bar{K} = K\Big(1 + (|\eta| + K(b-a))e^{K(b-a)}\Big)$.

Proof: Since the right-hand side function g is continuous and it is of at most linear growth (i.e. (G1) and (G2) are satisfied), Peano's theorem guarantees existence of the solution (e.g. see Theorem 70.4, page 292 in [34]). The uniqueness follows from the monotonicity condition (G3). Namely, let us assume that (39) has two solutions $z = z(t)$ and $x = x(t)$ with the same initial-value $z(a) = x(a) = \eta$. Then for all $t \in [a, b]$

$$\frac{d}{dt}(z(t) - x(t))^2 = 2(z(t) - x(t))(g(t, z(t)) - g(t, x(t))) \leq 0.$$

Therefore, the mapping $[a, b] \ni t \mapsto (z(t) - x(t))^2$ is non-increasing and we get for all $t \in [a, b]$

$$(z(t) - x(t))^2 \leq (z(a) - x(a))^2 = 0,$$

which, together with continuity of z, x, implies that $z(t) = x(t)$ for all $t \in [a, b]$.

For all $t \in [a, b]$ by (G2) we get

$$\begin{aligned} |z(t)| &\leq |\eta| + \int_a^t |g(s, z(s))|ds \\ &\leq |\eta| + K(b-a) + K\int_a^t |z(s)|ds, \end{aligned} \tag{42}$$

and by Gronwall's lemma we obtain (40). The estimate (41) follows from (G2), (40) and the mean value theorem. □

The following result provides an upper bound on the error of explicit Euler method applied to ODEs with monotone and Hölder continuous right-hand side functions.

Lemma 3.4: Let us consider the following ordinary differential equation

$$z'(t) = g(t, z(t)), \quad t \in [a, b], \quad z(a) = \eta, \tag{43}$$

where $-\infty < a < b < +\infty$, $\eta \in \mathbb{R}$ *and* $g : [a, b] \times \mathbb{R} \to \mathbb{R}$ *satisfies the following conditions*:

(G1) $g \in C([a, b] \times \mathbb{R}; \mathbb{R})$.

(G2) *There exists* $K > 0$ *such that for all* $(t, y) \in [a, b] \times \mathbb{R}$

$$|g(t, y)| \leq K(1 + |y|).$$

(G3) *For all* $t \in [a, b]$, $y_1, y_2 \in \mathbb{R}$

$$(y_1 - y_2)(g(t, y_1) - g(t, y_2)) \leq 0.$$

[1] $\mathrm{sgn}(x) = 1$ if $x \geq 0$ and $\mathrm{sgn}(x) = -1$ if $x < 0$.

(G4) *There exist* $L > 0$ *and* $\gamma_1, \gamma_2, \gamma_3 \in (0, 1]$ *such that for all* $t_1, t_2 \in [a, b]$, $y_1, y_2 \in \mathbb{R}$

$$|g(t_1, y_1) - g(t_2, y_2)| \leq L\Big((1 + |y_1| + |y_2|)|t_1 - t_2|^{\gamma_1} + |y_1 - y_2|^{\gamma_2} + |y_1 - y_2|^{\gamma_3}\Big).$$

Let us consider the explicit Euler method based on equidistant discretization. Namely, for $n \in \mathbb{N}$ *we set* $h = (b - a)/n$, $t_k = a + kh$, $k = 0, 1, \ldots, n$, *and let* $y_0 \in \mathbb{R}$ *be such that* $|\eta - y_0| \leq \Delta$. *We take*

$$y_{k+1} = y_k + h \cdot g(t_k, y_k), \quad k = 0, 1, \ldots, n-1. \tag{44}$$

Then the following holds.

(i) *There exists* $C_1 = C_1(a, b, K, \eta) > 0$ *such that for all* $n \in \mathbb{N}$, $\Delta \in [0, +\infty)$ *we have*

$$\max_{0 \leq k \leq n} |y_k| \leq C_1(1 + \Delta). \tag{45}$$

(ii) *There exists* $C_2 = C_2(a, b, L, K, \eta, \gamma_1, \gamma_2, \gamma_3) > 0$ *such that for all* $n \in \mathbb{N}$, $\Delta \in [0, +\infty)$ *we have*

$$\max_{0 \leq k \leq n} |z(t_k) - y_k| \leq C_2(\Delta + h^{\gamma_1} + h^{\gamma_2} + h^{\gamma_3}). \tag{46}$$

Proof: We have that

$$|y_{k+1}| \leq (1 + hK)|y_k| + hK, \quad k = 0, 1, \ldots, n-1 \tag{47}$$

and $|y_0| \leq |\eta| + \Delta$. Hence, by the discrete version of Gronwall's lemma we get that for all $k = 0, 1, \ldots, n$

$$|y_k| \leq e^{K(b-a)}(|\eta| + \Delta + 1) - 1 \leq C_1(1 + \Delta), \tag{48}$$

where $C_1 = \max\{e^{K(b-a)}(|\eta| + 1) - 1, e^{K(b-a)}\}$. This proves (45).

For $k = 0, 1, \ldots, n-1$ we consider the following local ordinary differential equation

$$z_k'(t) = g(t, z_k(t)), \quad t \in [t_k, t_{k+1}], \quad z_k(t_k) = y_k. \tag{49}$$

By (48) we get for all $t \in [t_k, t_{k+1}]$ that

$$|z_k(t)| \leq |y_k| + \int_{t_k}^{t} |g(s, z_k(s))|ds \leq C_1(1 + \Delta) + K(b - a) + K\int_{t_k}^{t} |z_k(s)|ds, \tag{50}$$

and by the Gronwall's lemma we obtain

$$\sup_{t \in [t_k, t_{k+1}]} |z_k(t)| \leq C_2(1 + \Delta), \tag{51}$$

where $C_2 = (C_1 + K(b - a))e^{K(b-a)}$. Therefore, for all $t \in [t_k, t_{k+1}]$

$$|z_k(t) - y_k| \leq \int_{t_k}^{t} |g(s, z_k(s))|ds \leq hK\Big(1 + \sup_{t \in [t_k, t_{k+1}]} |z_k(t)|\Big) \leq C_3(1 + \Delta)h, \tag{52}$$

with $C_3 = (1 + C_2)K$. Now, we have that

$$|z(t_{k+1}) - y_{k+1}| \leq |z(t_{k+1}) - z_k(t_{k+1})| + |z_k(t_{k+1}) - y_{k+1}|, \tag{53}$$

for $k = 0, 1, \ldots, n-1$. Note that for all $t \in [t_k, t_{k+1}]$, due to the assumption (G3), the following holds

$$\begin{aligned}(z(t) - z_k(t))^2 &= (z(t_k) - y_k)^2 \\ &\quad + 2 \cdot \int_{t_k}^{t} (z(s) - z_k(s))\,(g(s, z(s)) - g(s, z_k(s)))\,ds \\ &\leq (z(t_k) - y_k)^2.\end{aligned} \tag{54}$$

Hence, we arrive at

$$|z(t_{k+1}) - z_k(t_{k+1})| \leq |z(t_k) - y_k|. \tag{55}$$

We now estimate the second term in (53). We have by (44), (48), (49), (51), (G4), and (52) that

$$\begin{aligned}&|z_k(t_{k+1}) - y_{k+1}| \\ &= \Big|z_k(t_k) - y_k + \int_{t_k}^{t_{k+1}} \Big(g(s, z_k(s)) - g(t_k, y_k)\Big)ds\Big| \\ &\leq \int_{t_k}^{t_{k+1}} |g(s, z_k(s)) - g(t_k, y_k)|ds \\ &\leq L\int_{t_k}^{t_{k+1}} \Big((1 + |z_k(s)| + |y_k|)|s - t_k|^{\gamma_1} \\ &\quad + |z_k(s) - y_k|^{\gamma_2} + |z_k(s) - y_k|^{\gamma_3}\Big)ds \\ &\leq \tilde{C}_4 h\Big((1 + \Delta)h^{\gamma_1} + (1 + \Delta)^{\gamma_2}h^{\gamma_2} + (1 + \Delta)^{\gamma_3}h^{\gamma_3}\Big),\end{aligned} \tag{56}$$

where $\tilde{C}_4 = L\max\{(1 + C_1 + C_2)/(1 + \gamma_1), C_3^{\gamma_2}, C_3^{\gamma_3}\}$. Since $(1 + \Delta)^{\gamma_i} \leq 2(1 + \Delta)$, $i = 1, 2$, we obtain that

$$|z_k(t_{k+1}) - y_{k+1}| \leq C_4 h(1 + \Delta)(h^{\gamma_1} + h^{\gamma_2} + h^{\gamma_3}), \tag{57}$$

where $C_4 = 2L\tilde{C}_4$.

Let us denote

$$e_k = z(t_k) - y_k, \quad k = 0, 1, \ldots, n. \tag{58}$$

Of course $|e_0| \leq \Delta$. By (53), (55), and (57) we have the following recursive inequality

$$|e_{k+1}| \leq |e_k| + C_4(1+\Delta)h(h^{\gamma_1} + h^{\gamma_2} + h^{\gamma_3}), \tag{59}$$

for $k = 0, 1, \ldots, n-1$. It is easy to see that

$$\begin{aligned} |e_k| &\leq \Delta + kC_4(1+\Delta)h(h^{\gamma_1} + h^{\gamma_2} + h^{\gamma_3}) \\ &\leq \Delta + C_4(b-a)(h^{\gamma_1} + h^{\gamma_2} + h^{\gamma_3}), \qquad (60) \\ &\leq C(\Delta + h^{\gamma_1} + h^{\gamma_2} + h^{\gamma_3}), \qquad (61) \end{aligned}$$

for all $k = 0, 1, \ldots, n$, where $C = 6(1+b-a)\max\{1, (b-a)C_4\}$. This ends the proof of (46), completing the proof of lemma. □

In the following lemma we show, by using the results above, that the delay differential equation (30) has unique solution under assumptions (F1)-(F3). Note that the assumptions are weaker than those known from the standard literature. Namely, we use only monotonicity and local Hölder condition for the right-hand side function f.

Lemma 3.5: Let $\eta \in \mathbb{R}$ and let f satisfy (F1)-(F3). Then the equation (30) has a unique continuously differentiable solution that exists for any $t \geq 0$. Moreover, if we denote by $\phi_n = \phi_n(t)$ the solution of (30) on the interval $[nt_{cr}, (n+1)t_{cr}]$, then for all $n \in \mathbb{N}_0$ there exist $K_0, K_1, \ldots, K_n \geq 0$ such that

$$\sup_{nt_{cr} \leq t \leq (n+1)t_{cr}} |\phi_n(t)| \leq K_n, \tag{62}$$

and, for all $t, s \in [nt_{cr}, (n+1)t_{cr}]$

$$|\phi_n(t) - \phi_n(s)| \leq \bar{K}_n |t-s|, \tag{63}$$

with $\bar{K}_n = K(1+K_{n-1})(1+K_n)$, where $K_{-1} := |\eta|$.

Proof: We proceed by induction with respect to n.

For $n = 0$, the equation (30) can be written as

$$z'(t) = f(t, z(t), \eta), \quad t \in [0, t_{cr}], \tag{64}$$

with the initial condition $z(0) = \eta$. Denoting by

$$g_0(t, y) = f(t, y, \eta), \quad t \in [0, t_{cr}], y \in \mathbb{R}, \tag{65}$$

we get, by the properties of f, that $g_0 \in C([0, t_{cr}] \times \mathbb{R})$,

$$|g_0(t, y)| \leq \hat{K}_0(1 + |y|), \tag{66}$$

with $\hat{K}_0 = K(1 + |\eta|)$, and

$$(y_1 - y_2)(g_0(t, y_1) - g_0(t, y_2)) \leq 0, \quad \text{for all } y_1, y_2 \in \mathbb{R}. \tag{67}$$

Therefore, by Lemma 3.3 we get that there exists a unique continuously differentiable solution $\phi_0 : [0, t_{cr}] \to \mathbb{R}$ of the equation (64), such that

$$\sup_{t \in [0, t_{cr}]} |\phi_0(t)| \leq K_0,$$

where

$$\begin{aligned} K_0 &= (|\eta| + \hat{K}_0 t_{cr}) e^{\hat{K}_0 t_{cr}} \\ &= (|\eta| + K(1 + |\eta|)t_{cr}) e^{K(1+|\eta|)t_{cr}} \geq 0, \end{aligned}$$

and for all $t, s \in [0, t_{cr}]$

$$|\phi_0(t) - \phi_0(s)| \leq \bar{K}_0 |t-s|,$$

where

$$\bar{K}_0 = \hat{K}_0(1 + K_0) = K(1 + K_{-1})(1 + K_0)$$

depends only on η, K, t_{cr}.

Let us now assume that there exists $n \in \mathbb{N}_0$ such that the statement of the lemma holds for the solution $\phi_n : [nt_{cr}, (n+1)t_{cr}] \to \mathbb{R}$. Consider the equation

$$z'(t) = f(t, z(t), \phi_n(t - t_{cr})), \quad t \in [(n+1)t_{cr}, (n+2)t_{cr}], \tag{68}$$

with the initial condition $z((n+1)t_{cr}) = \phi_n((n+1)t_{cr})$. Let

$$\begin{aligned} g_{n+1}(t, y) &= f(t, y, \phi_n(t - t_{cr})), \\ & t \in [(n+1)t_{cr}, (n+2)t_{cr}], y \in \mathbb{R}. \end{aligned} \tag{69}$$

We get by the inductive assumption and from the properties of f that $g_{n+1} \in C([(n+1)t_{cr}], (n+2)t_{cr}] \times \mathbb{R}; \mathbb{R})$, for all $y \in \mathbb{R}$ we have

$$\begin{aligned} |g_{n+1}(t, y)| &\leq K\left(1 + \sup_{nt_{cr} \leq t \leq (n+1)t_{cr}} |\phi_n(t)|\right)(1 + |y|) \\ &\leq \hat{K}_{n+1}(1 + |y|), \end{aligned} \tag{70}$$

with $\hat{K}_{n+1} = K(1 + K_n)$, and

$$(y_1 - y_2)(g_{n+1}(t, y_1) - g_{n+1}(t, y_2)) \leq 0, \quad y_1, y_2 \in \mathbb{R}. \tag{71}$$

Hence, again by Lemma 3.3 we get that there exists a unique continuously differentiable solution $\phi_{n+1} : [(n+1)t_{cr}, (n+2)t_{cr}] \to \mathbb{R}$ of the equation (68), such that

$$\begin{aligned} &\sup_{t \in [(n+1)t_{cr}, (n+2)t_{cr}]} |\phi_{n+1}(t)| \leq K_{n+1}, \\ K_{n+1} &= (K_n + \hat{K}_{n+1} t_{cr}) e^{\hat{K}_{n+1} t_{cr}} \\ &= (K_n + K(1 + K_n)t_{cr}) e^{K(1+K_n)t_{cr}} \geq 0, \end{aligned}$$

where and for all $t, s \in [(n+1)t_{cr}, (n+2)t_{cr}]$ we have

$$|\phi_{n+1}(t) - \phi_{n+1}(s)| \leq \bar{K}_{n+1} |t-s|,$$

where $\bar{K}_{n+1} = \hat{K}_{n+1}(1 + K_{n+1}) = K(1 + K_n)(1 + K_{n+1})$.

From the above inductive construction we see that the solution of (30) is continuous. Moreover, due to the continuity of f, ϕ_n, and ϕ_{n-1} we get for any $n \in \mathbb{N}_0$ that

$$\begin{aligned} &\lim_{t \to (n+1)t_{cr}-} z'(t) \\ &= \lim_{t \to (n+1)t_{cr}-} \phi_n'(t) \\ &= \lim_{t \to (n+1)t_{cr}-} f(t, \phi_n(t), \phi_{n-1}(t - t_{cr})) \\ &= f((n+1)t_{cr}, \phi_n((n+1)t_{cr}), \phi_{n-1}(nt_{cr})) \\ &= f((n+1)t_{cr}, \phi_{n+1}((n+1)t_{cr}), \phi_n(nt_{cr})) \\ &= \lim_{t \to (n+1)t_{cr}+} f(t, \phi_{n+1}(t), \phi_n(t - t_{cr})) \\ &= \lim_{t \to (n+1)t_{cr}+} \phi_{n+1}'(t) = \lim_{t \to (n+1)t_{cr}+} z'(t). \end{aligned}$$

Hence, the solution of (30) is continuously differentiable.

The proof is completed. □

Lemma 3.6: Let $\eta \in \mathbb{R}$ and let f satisfy (F1)-(F4). For any $n \in \mathbb{N}_0$ consider the function $g_n : [nt_{cr}, (n+1)t_{cr}] \times \mathbb{R} \to \mathbb{R}$ given by

$$g_n(t, y) = f(t, y, \phi_{n-1}(t - t_{cr})), \tag{72}$$

where $\phi_n = \phi_{n-1}(t)$ is the solution of (30) on the interval $[(n-1)t_{cr}, nt_{cr}]$ and $\phi_{-1}(t) := \eta$ for all $t \in [-t_{cr}, 0]$. Then

(i) $g_n \in C([nt_{cr}, (n+1)t_{cr}] \times \mathbb{R}; \mathbb{R})$.

(ii) *For all $(t, y) \in [nt_{cr}, (n+1)t_{cr}] \times \mathbb{R}$*

$$|g_n(t, y)| \le \hat{K}_n(1 + |y|),$$

where $K_{-1} = |\eta|$, $\hat{K}_n = K(1 + K_{n-1})$ and K_{n-1} is the constant from Lemma 3.5.

(iii) *For all $t \in [nt_{cr}, (n+1)t_{cr}]$, $y_1, y_2 \in \mathbb{R}$*

$$(y_1 - y_2)(g_n(t, y_1) - g_n(t, y_2)) \le 0.$$

(iv) *For all $t_1, t_2 \in [nt_{cr}, (n+1)t_{cr}]$, $y_1, y_2 \in \mathbb{R}$*

$$\begin{aligned} &|g_n(t_1, y_1) - g_n(t_2, y_2)| \\ &\quad \le \hat{L}_n\Big((1 + |y_1| + |y_2|) \cdot |t_1 - t_2|^\alpha \\ &\qquad + |y_1 - y_2|^\beta + |y_1 - y_2|^\gamma\Big), \end{aligned}$$

where $\hat{L}_n = L(1 + 2K_{n-1} + t_{cr}^{1-\alpha}\bar{K}_{n-1})$ and $\bar{K}_{-1} := 0$, $K_{-1} := |\eta|$.

Proof: Conditions (i), (ii), and (iii) follow by Lemma 3.5.

By the assumption (F4) and Lemma 3.5 we get for all $t_1, t_2 \in [nt_{cr}, (n+1)t_{cr}]$, $y_1, y_2 \in \mathbb{R}$ that

$$\begin{aligned} &|g_n(t_1, y_1) - g_n(t_2, y_2)| \\ &= |f(t_1, y_1, \phi_{n-1}(t_1 - t_{cr})) - f(t_2, y_2, \phi_{n-1}(t_2 - t_{cr}))| \\ &\le L\Big((1 + |y_1| + |y_2|) \cdot (1 + |\phi_{n-1}(t_1 - t_{cr})| \\ &\quad + |\phi_{n-1}(t_2 - t_{cr})|) \cdot |t_1 - t_2|^\alpha + |y_1 - y_2|^\beta \\ &\quad + (1 + |\phi_{n-1}(t_1 - t_{cr})| + |\phi_{n-1}(t_2 - t_{cr})|) \cdot |y_1 - y_2|^\gamma \\ &\quad + (1 + |y_1| + |y_2|) \cdot |\phi_{n-1}(t_1 - t_{cr}) - \phi_{n-1}(t_2 - t_{cr})|\Big) \\ &\le L\Big((1 + |y_1| + |y_2|) \cdot (1 + 2K_{n-1}) \cdot |t_1 - t_2|^\alpha \\ &\quad + |y_1 - y_2|^\beta + (1 + 2K_{n-1}) \cdot |y_1 - y_2|^\gamma \\ &\quad + \bar{K}_{n-1}(1 + |y_1| + |y_2|) \cdot |t_1 - t_2|\Big) \\ &\le \hat{L}_n\Big((1 + |y_1| + |y_2|) \cdot |t_1 - t_2|^\alpha + |y_1 - y_2|^\beta + |y_1 - y_2|^\gamma\Big). \end{aligned}$$

□

Now we are ready to prove Theorem 3.2.

Proof of Theorem 3.2: On the interval $[0, t_{cr}]$ we approximate the solution of (30) by the explicit Euler method

$$y_0^0 = \eta, \tag{73}$$

$$y_{k+1}^0 = y_k^0 + h \cdot g_0(t_k^0, y_k^0), \quad k = 0, 1, \ldots, N-1, \tag{74}$$

where $g_0(t, y) = f(t, y, \eta)$. Applying Lemmas 3.6 and 3.4 to $\eta := \eta$, $g := g_0$, $[a, b] := [0, t_{cr}]$, $\Delta := 0$ we get that

$$\max_{0 \le k \le N} |\phi_0(t_k^0) - y_k^0| \le C_0(h^\alpha + h^\beta + h^\gamma), \tag{75}$$

where $C_0 = C_0(t_{cr}, L, K, \eta, \alpha, \beta, \gamma) \ge 0$, and

$$|y_k^0| \le \tilde{K}_0, \quad k = 0, 1, \ldots, N, \tag{76}$$

where $\tilde{K}_0 = \tilde{K}_0(t_{cr}, K, \eta) \ge 0$.

In $[t_{cr}, 2t_{cr}]$ we consider the following differential equation

$$z'(t) = g_1(t, z(t)), \quad t \in [t_{cr}, 2t_{cr}], \tag{77}$$

with the initial value $z(t_{cr}) = \phi_0(t_{cr}) = \phi_0(t_N^0)$ and $g_1(t, y) = f(t, y, \phi_0(t - t_{cr}))$. We approximate (77) by the auxiliary Euler scheme

$$\tilde{y}_0^1 := y_0^1 = y_N^0, \tag{78}$$

$$\tilde{y}_{k+1}^1 = \tilde{y}_k^1 + h \cdot g_1(t_k^1, \tilde{y}_k^1), \quad k = 0, 1, \ldots, N-1. \tag{79}$$

By (75) we have that

$$|\phi_1(t_0^1) - \tilde{y}_0^1| = |\phi_0(t_N^0) - y_N^0| \le C_0(h^\alpha + h^\beta + h^\gamma). \tag{80}$$

Applying Lemmas 3.6, 3.5 and 3.4 to $\eta := \phi_0(t_N^0)$, $g := g_1$, $[a, b] := [t_{cr}, 2t_{cr}]$, $\Delta := C_0(h^\alpha + h^\beta + h^\gamma)$ we get that

$$|\phi_0(t_N^0)| \le K_0, \tag{81}$$

and

$$\max_{0 \le k \le N} |\phi_1(t_k^1) - \tilde{y}_k^1| \le \tilde{C}_1(h^\alpha + h^\beta + h^\gamma), \tag{82}$$

where $\tilde{C}_1 = \tilde{C}_1(t_{cr}, L, K, \eta, \alpha, \beta, \gamma) \ge 0$ that, in particular, depends on the initial value η of the equation (30). Let us denote by

$$e_k^1 = \tilde{y}_k^1 - y_k^1, \quad k = 0, 1, \ldots, N,$$

where we have that $e_0^1 = \tilde{y}_0^1 - y_0^1 = 0$. From (79) and (35) we have for $k = 0, 1, \ldots, N-1$ that

$$e_{k+1}^1 = e_k^1 + h\mathcal{R}_k^1 + h\mathcal{L}_k^1, \tag{83}$$

where

$$\mathcal{R}_k^1 = f(t_k^1, \tilde{y}_k^1, \phi_0(t_k^0)) - f(t_k^1, y_k^1, \phi_0(t_k^0))$$

and

$$\mathcal{L}_k^1 = f(t_k^1, y_k^1, \phi_0(t_k^0)) - f(t_k^1, y_k^1, y_k^0).$$

From (83) we obtain that

$$(e_{k+1}^1 - h\mathcal{L}_k^1)^2 = (e_k^1 + h\mathcal{R}_k^1)^2,$$

which, together with the assumption (F3), implies

$$\begin{aligned} (e_{k+1}^1)^2 &\le (e_k^1)^2 + h^2(\mathcal{R}_k^1)^2 + 2he_{k+1}^1\mathcal{L}_k^1, \\ &k = 0, 1, \ldots, N-1. \end{aligned} \tag{84}$$

Moreover,

$$e^1_{k+1}\mathcal{L}^1_k \le \frac{1}{2}\Big((e^1_{k+1})^2 + (\mathcal{L}^1_k)^2\Big),$$

hence

$$(e^1_{k+1})^2 \le (e^1_k)^2 + h^2(\mathcal{R}^1_k)^2 + h(e^1_{k+1})^2 + h(\mathcal{L}^1_k)^2, \quad k = 0, 1, \ldots, N-1. \tag{85}$$

Since $0 < 1/(1-h) \le 1 + 2h \le 2$ for $h \in (0, 1/2)$, we have that

$$(e^1_{k+1})^2 \le (1+2h)(e^1_k)^2 + 2h^2(\mathcal{R}^1_k)^2 + 2h(\mathcal{L}^1_k)^2, \quad k = 0, 1, \ldots, N-1. \tag{86}$$

Recall a well known fact that for all $\varrho \in (0, 1]$ and $x \in \mathbb{R}$ it holds

$$|x|^\varrho \le 1 + |x|. \tag{87}$$

Then by the assumption (F4), Lemma 3.5 and (75) we have the following estimates

$$|\mathcal{R}^1_k| \le L\Big(|e^1_k|^\beta + (1+2\sup_{0\le t\le t_{cr}}|\phi_0(t)|)\cdot|e^1_k|^\gamma\Big) \le c_1(1+|e^1_k|), \tag{88}$$

where $c_1 = c_0(L, K_0) \ge 0$, and

$$\begin{aligned}|\mathcal{L}^1_k| &\le L(1+2|y^1_k|)\cdot|\phi_0(t^0_k) - y^0_k| \\ &\le LC_0(1+2|y^1_k|)(h^\alpha + h^\beta + h^\gamma).\end{aligned} \tag{89}$$

Furthermore, it holds that for all $k = 0, 1, \ldots, N-1$

$$\begin{aligned}|y^1_{k+1}| &\le |y^1_k| + h\cdot|f(t^1_k, y^1_k, y^0_k)| \\ &\le |y^1_k| + hK(1+|y^1_k|)(1+|y^0_k|) \\ &\le |y^1_k| + hK(1+\tilde{K}_0)(1+|y^1_k|) \\ &= (1+h\tilde{c}_1)|y^1_k| + h\tilde{c}_1,\end{aligned}$$

where $\tilde{c}_1 = \tilde{c}_1(K, \tilde{K}_0) \ge 0$ and $|y^1_0| = |y^0_N| \le \tilde{K}_0$. By using discrete Gronwall's inequality we obtain

$$|y^1_k| \le \tilde{K}_1, \quad k = 0, 1, \ldots, N. \tag{90}$$

Therefore, by (90) and (89) we obtain for all $k = 0, 1, \ldots, N$

$$|\mathcal{L}^1_k| \le \bar{c}_1(h^\alpha + h^\beta + h^\gamma), \tag{91}$$

with $\bar{c}_1$ independent of N. From (86), (88), and (91) we get for sufficiently large N and $k = 0, 1, \ldots, N-1$ that

$$(e^1_{k+1})^2 \le (1+3h)(e^1_k)^2 + D_1h^2 + D_2h(h^{2\alpha} + h^{2\beta} + h^{2\gamma}), \tag{92}$$

where $D_1, D_2 \ge 0$ are independent of N. Solving this discrete inequality yields

$$(e^1_k)^2 \le \bar{D}_1(h + h^{2\alpha} + h^{2\beta} + h^{2\gamma}), \quad k = 0, 1, \ldots, N, \tag{93}$$

with $\bar{D}_1 \ge 0$ independent of N. Since

$$|\phi_1(t^1_k) - y^1_k| \le |\phi_1(t^1_k) - \tilde{y}^1_k| + |e^1_k|,$$

by (82) and (93), we arrive at

$$\max_{0\le k\le N}|\phi_1(t^1_k) - y^1_k| \le C_1(h^{1/2} + h^\alpha + h^\beta + h^\gamma), \tag{94}$$

with $C_1 \ge 0$ independent of N.

On the consecutive intervals we proceed by induction. Namely, let us assume that there exist $1 \le j \le n-1$ and $C_j, \tilde{K}_j \ge 0$ such that

$$\max_{0\le k\le N}|\phi_j(t^j_k) - y^j_k| \le C_j(h^{1/2} + h^\alpha + h^\beta + h^\gamma), \tag{95}$$

and

$$|y^j_k| \le \tilde{K}_j, \quad k = 0, 1, \ldots, N. \tag{96}$$

(For $j = 1$ the statement has already been proven in (94) and (90).) In the interval $[(j+1)t_{cr}, (j+2)t_{cr}]$ we consider the following ODE

$$z'(t) = g_{j+1}(t, z(t)), \quad t \in [(j+1)t_{cr}, (j+2)t_{cr}], \tag{97}$$

with the initial value $z((j+1)t_{cr}) = \phi_{j+1}((j+1)t_{cr}) = \phi_j(t^{j+1}_0)$ and $g_{j+1}(t, y) = f(t, y, \phi_j(t - t_{cr}))$. We approximate (97) by the following auxiliary Euler scheme

$$\tilde{y}^{j+1}_0 := y^{j+1}_0 = y^j_N, \tag{98}$$

$$\tilde{y}^{j+1}_{k+1} = \tilde{y}^{j+1}_k + h\cdot g_{j+1}(t^{j+1}_k, \tilde{y}^{j+1}_k), \quad k = 0, 1, \ldots, N-1. \tag{99}$$

By (95) we have that

$$\begin{aligned}|\phi_{j+1}(t^{j+1}_0) - \tilde{y}^{j+1}_0| &= |\phi_j(t^j_N) - y^j_N| \\ &\le C_j(h^{1/2} + h^\alpha + h^\beta + h^\gamma).\end{aligned} \tag{100}$$

Repeating the arguments used from (77) to (94), but now for $\eta := \phi_j(t^{j+1}_0)$, $g := g_{j+1}$, $[a, b] := [(j+1)t_{cr}, (j+2)t_{cr}]$, $\Delta := C_j(h^{1/2} + h^\alpha + h^\beta + h^\gamma)$, we obtain

$$|\phi_j(t^{j+1}_0)| = |\phi_j(t^j_N)| \le K_j, \tag{101}$$

and

$$\begin{aligned}&\max_{0\le k\le N}|\phi_{j+1}(t^{j+1}_k) - y^{j+1}_k| \\ &\le \max_{0\le k\le N}|\phi_{j+1}(t^{j+1}_k) - \tilde{y}^{j+1}_k| + \max_{0\le k\le N}|\tilde{y}^{j+1}_k - y^{j+1}_k| \\ &\le C_{j+1}(h^{1/2} + h^\alpha + h^\beta + h^\gamma),\end{aligned} \tag{102}$$

and

$$|y^{j+1}_k| \le \tilde{K}_{j+1}, \quad k = 0, 1, \ldots, N, \tag{103}$$

with $\tilde{K}_{j+1}, C_{j+1} \ge 0$ independent of N, provided that N is sufficiently large. This ends the proof. □

Remark 3.7: In Lemma 3.1 we provided an example of a function $\tilde{f}$ that satisfies (F1)-(F4). Note that $\tilde{f}$, with $A(t) = A_1(t)\cdot\dot{\varepsilon}(t)$, $B(t) = A_2(t)\cdot\dot{\varepsilon}(t)^{1-a_9}$, $C(t) = A_3(t)$, coincides in $[t_{cr}, +\infty)\times[0, +\infty)\times[0, +\infty)$ with

$$f(t, y, z) = A(t) - B(t)\cdot y - C(t)\cdot y^{a_8}\cdot z, \quad t \ge t_{cr}, y \ge 0, z \ge 0, \tag{104}$$

which is a right-hand side function of the main equation (2) *for* $t \geq t_{cr}$ *where* z *represents the delay term* $\mathcal{R}(t - t_{cr})$. *Knowing that the solution* ρ *of* (2) *is unique and non-negative (see Theorem 2.6), the solutions of* (2) *and*

$$\tilde{\rho}'(t) = \tilde{f}(t, \tilde{\rho}(t), \tilde{\rho}(t - t_{cr})), \tag{105}$$

coincide for $t \geq t_{cr}$. *(We take* $\tilde{\rho}(t) = \rho(t)$ *for* $t \in [-t_{cr}, t_{cr}]$.*) This justifies, why we can use the Euler scheme in order to approximate the nonnegative solution* ρ *of* (2).

IV. NUMERICAL EXPERIMENTS

In this section we will provide numerical simulations of (2) with real world parameters. We have conducted the experiments with our own C++ implementation of the method mentioned above. Additionally, all floating point numbers was kept as a double data type. However, before we dive into the test results of (2), we will take a closer look to (8), that is we assume that A_i and $\dot{\varepsilon}$ are time independent. This will give us a preliminary insight into possible evolution of (2). In particular we will see how it changes with the change of parameters A_i, in particular influence of the boundary condition A_1/A_2. We will also check how the accuracy of solutions changes with time step, and comment of empirical speed of convergence of numerical solutions.

It is also worth mentioning that (8), while much simplified compared to (2), has its utility for modeling of our process. Namely, it can be used in inverse analysis, as laboratory experiments are usually done in controlled environment. In particular T and $\dot{\varepsilon}$ can be assumed constant in laboratory experiments, which leads to time-independent coefficients $A_i(t) \equiv A_i$.

A. EMPIRICAL TESTS OF CONVERGENCE - SELECTED INSTANCES OF EQUATION (8)

As before, we divide our discussion into two cases when $a_8 \in \{0, 1\}$.

In the case when $\mathbf{a_8 = 0}$, we consider four sets of parameters (see Fig. 2)

(a) $\rho_0 = 0, \rho_{cr} = 1, A_1 = 10, A_2 = 1, A_3 = 0.9$,
(b) $\rho_0 = 0, \rho_{cr} = 4, A_1 = 10, A_2 = 2, A_3 = 1$,
(c) $\rho_0 = 0, \rho_{cr} = 9, A_1 = 10, A_2 = 1, A_3 = 0.9$.

All solutions are considered on the interval $[0, 10\ t_{cr}]$. Initial conditions on all particular intervals are given by values of corresponding analytical formula.

We also considered case $\mathbf{a_8 = 0}$ with parameters range showing influence of violated condition A_2/A_3 (see Fig. 3):

(d) $\rho_0 = 0, \rho_{cr} = 9, A_1 = 10, A_2 = 1, A_3 \in [0.9; 1.5]$,
(e) $\rho_0 = 0, \rho_{cr} = 4, A_1 = 10, A_2 = 1, A_3 \in [0.5; 5]$.

Note, that in these cases $\frac{A_3}{A_2} = 1$ or we even have $\frac{A_3}{A_2} > 1$. Let us emphasize, that the assumptions of Theorem 2.2 are broken. Nevertheless, the derived methods work properly what suggests that the assumptions might be weakened in further research. Notice however, that while solutions exists (and can be computed), it is hard to find their technological justification (recall that ρ represents dislocation density, so Fig. 3(e) definitely cannot represent real technological process). Note that similarly to effect observed in [32] for equation similar to the case $a_8 = 0$, large $A_3/A_2 > 1$ (or large t_{cr}) may lead to unbounded oscillations of solutions and technologically unjustified solutions. In fact, as we can see, such solutions may occur even when solution stabilizes (i.e. oscillations are bounded and decreasing in amplitude).

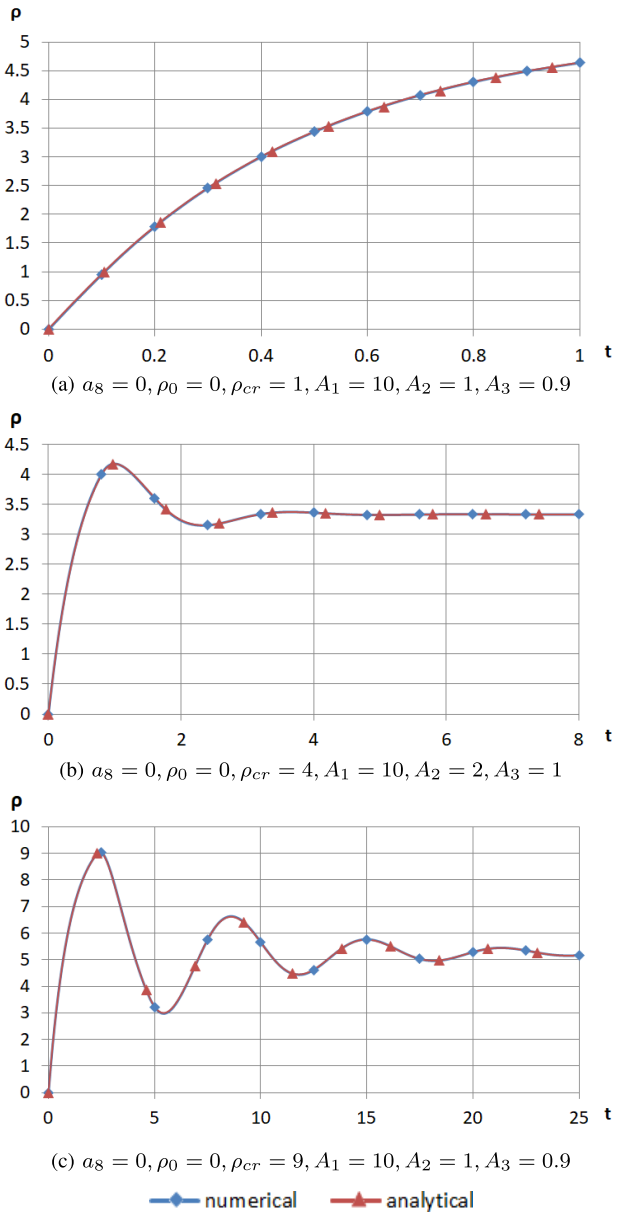

(a) $a_8 = 0, \rho_0 = 0, \rho_{cr} = 1, A_1 = 10, A_2 = 1, A_3 = 0.9$

(b) $a_8 = 0, \rho_0 = 0, \rho_{cr} = 4, A_1 = 10, A_2 = 2, A_3 = 1$

(c) $a_8 = 0, \rho_0 = 0, \rho_{cr} = 9, A_1 = 10, A_2 = 1, A_3 = 0.9$

FIGURE 2. Exemplary analytical and numerical solutions in the case when $a_8 = 0$.

In the case when $\mathbf{a_8 = 1}$, we consider two exemplary sets of parameters (see Fig. 4):

(f) $\rho_0 = 0, \rho_{cr} = 4, A_1 = 10, A_2 = 2, A_3 = 1$,
(g) $\rho_0 = 0, \rho_{cr} = 9, A_1 = 10, A_2 = 1, A_3 = 0.9$.

Computing solution in consecutive intervals requires approximating of non elementary integrals. Therefore, the recursive formula for analytical solution, even for the third interval $[2t_{cr}, 3\ t_{cr}]$, is computationally very demanding

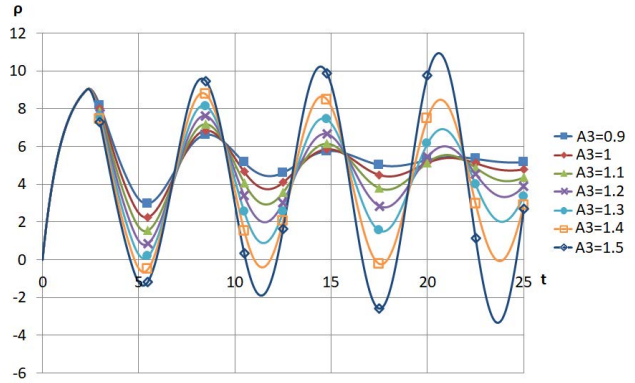

(d) $a_8 = 0, \rho_0 = 0, \rho_{cr} = 9, A_1 = 10, A_2 = 1$

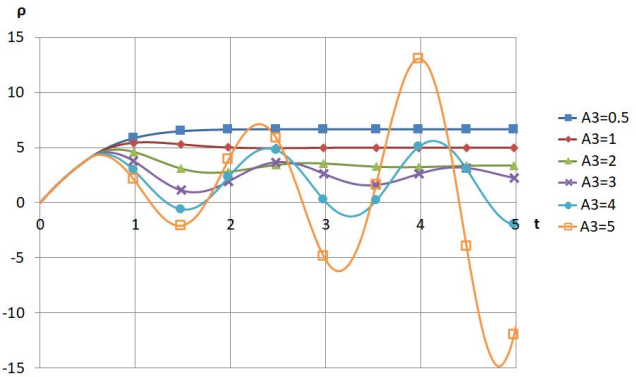

(e) $a_8 = 0, \rho_0 = 0, \rho_{cr} = 4, A_1 = 10, A_2 = 2, A_3 = 1$

FIGURE 3. Exemplary numerical solutions in the case when some assumptions are not satisfied.

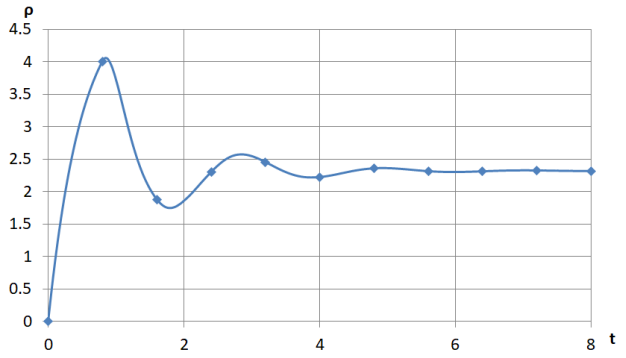

(f) $a_8 = 1, \rho_0 = 0, \rho_{cr} = 4, A_1 = 10, A_2 = 2, A_3 = 1$

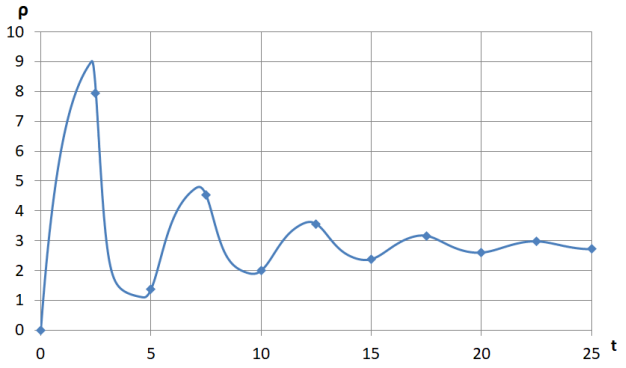

(g) $a_8 = 1, \rho_0 = 0, \rho_{cr} = 9, A_1 = 10, A_2 = 1, A_3 = 0.9$

FIGURE 4. Exemplary numerical solutions in the case when $a_8 = 1$.

(as the integrals needs to be approximated independently in each iteration). Because of that, for error comparison using the analytical solution, we restrict our attention only to the interval $[0, 2\ t_{cr}]$. Approximations by numerical methods, however, are computed for the whole considered interval $[0, 10t_{cr}]$. Then, the initial conditions for subsequent subintervals are taken from the numerical approximations.

In order to present numerical results of (8) we have to introduce some additional notations. Let $t_N = (t_0^1, t_1^1, \ldots, t_N^1, \ldots, t_N^m)$ be a vector of points, where $t_k^n = nt_{cr} + kh$, $k = 0, 1, \ldots, N$, $n = 1, 2, \ldots, m$, $h = \frac{t_{cr}}{N}$, and $m \in \mathbb{N}$. For given parameters of (8), we denote by $z_N = (z_0^1, z_1^1, \ldots, z_N^1, \ldots, z_N^m)$ a vector of values of exact solution of (8) computed in t_N points. Let ϕ be explicit Euler, backward Euler or Runge-Kutta scheme, see [23]. For each set of parameters we tracked the behavior of the worst case error, estimated by

$$\sup_{0\le k\le N, 1\le n\le m} |\phi(t_k^n) - z_k^n|, \quad h = \frac{t_{cr}}{N}, \tag{106}$$

as $N \to \infty$. Results of numerical tests are presented for case (b) in Fig. 5 and Table 1, and for case (g) in Fig. 6 and Table 2, where points of consecutive iterations of the method are depicted by dots. As we can see, the case of $a_8 = 1$ requires more delicate analysis for choosing N, because too small number leads to having points not reflecting properly the dynamics of solutions.

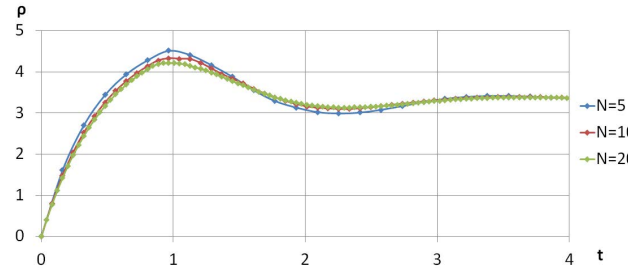

FIGURE 5. Numerical test for case (b) $a_8 = 0$, $\rho_0 = 0$, $\rho_{cr} = 4$, $A_1 = 10$, $A_2 = 2$, $A_3 = 1$ by explicit Euler method. Dots represent consecutive steps of the method.

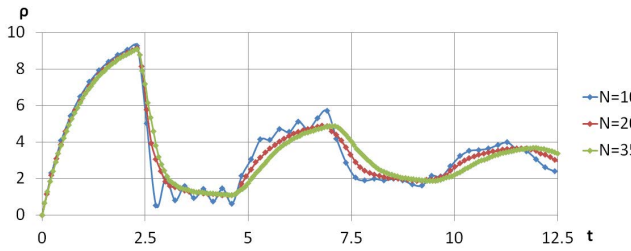

FIGURE 6. Numerical test for case (g) $a_8 = 1$, $\rho_0 = 0$, $\rho_{cr} = 9$, $A_1 = 10$, $A_2 = 1$, $A_3 = 0.9$ by explicit Euler method. Dots represent consecutive steps of the method.

In all the cases where assumption $\frac{A_3}{A_2} < 1$ is satisfied, viz. (a)-(c), (f)-(g) we observe the theoretical convergence rate.

TABLE 1. Error behavior for case (b) $a_8 = 0$, $\rho_0 = 0$, $\rho_{cr} = 4, A_1 = 10, A_2 = 2, A_3 = 1$.

N	$5 \cdot 1$	$5 \cdot 2$	$5 \cdot 3$	$5 \cdot 4$	$5 \cdot 5$
explicit Euler	$1.59 \cdot 10^{-1}$	$1.59 \cdot 10^{-1}$	$1.03 \cdot 10^{-1}$	$7.66 \cdot 10^{-1}$	$6.08 \cdot 10^{-2}$
backward Euler	$1.39 \cdot 10^{-1}$	$1.39 \cdot 10^{-1}$	$9.44 \cdot 10^{-2}$	$7.16 \cdot 10^{-2}$	$5.77 \cdot 10^{-2}$
RK4	$1.18 \cdot 10^{-5}$	$1.18 \cdot 10^{-5}$	$2.22 \cdot 10^{-6}$	$6.87 \cdot 10^{-7}$	$2.78 \cdot 10^{-7}$

N	$5 \cdot 6$	$5 \cdot 7$	$5 \cdot 8$	$5 \cdot 9$	$5 \cdot 10$
explicit Euler	$5.05 \cdot 10^{-2}$	$4.31 \cdot 10^{-2}$	$3.76 \cdot 10^{-2}$	$3.34 \cdot 10^{-2}$	$3.00 \cdot 10^{-2}$
backward Euler	$4.83 \cdot 10^{-2}$	$4.15 \cdot 10^{-2}$	$3.64 \cdot 10^{-2}$	$3.24 \cdot 10^{-2}$	$2.92 \cdot 10^{-2}$
RK4	$1.33 \cdot 10^{-7}$	$7.12 \cdot 10^{-8}$	$4.15 \cdot 10^{-8}$	$2.58 \cdot 10^{-8}$	$1.69 \cdot 10^{-8}$

N	10^2	10^3	10^4
explicit Euler	$1.49021416 \cdot 10^{-2}$	$1.48119132 \cdot 10^{-3}$	$1.48029707 \cdot 10^{-4}$
backward Euler	$1.47033478 \cdot 10^{-2}$	$1.47920577 \cdot 10^{-3}$	$1.48009854 \cdot 10^{-4}$
RK4	$1.04235599 \cdot 10^{-9}$	$1.03390588 \cdot 10^{-13}$	$6.00819550 \cdot 10^{-16}$

TABLE 2. Error behavior for case (g) $a_8 = 1$, $\rho_0 = 0$, $\rho_{cr} = 9, A_1 = 10, A_2 = 1, A_3 = 0.9$.

N	$5 \cdot 1$	$5 \cdot 2$	$5 \cdot 3$	$5 \cdot 4$	$5 \cdot 5$
explicit Euler	7.21	5.69	6.48	7.40	7.99
backward Euler	6.68	5.06	6.48	7.40	7.99
RK4	$3.18 \cdot 10^{-2}$	$3.18 \cdot 10^{-2}$	$4.70 \cdot 10^{-3}$	$1.29 \cdot 10^{-3}$	$4.95 \cdot 10^{-4}$

N	$5 \cdot 6$	$5 \cdot 7$	$5 \cdot 8$	$5 \cdot 9$	$5 \cdot 10$
explicit Euler	7.83	7.48	6.22	3.39	$2.48 \cdot 10^{-1}$
backward Euler	7.82	7.41	6.12	3.54	$2.31 \cdot 10^{-1}$
RK4	$2.26 \cdot 10^{-4}$	$1.17 \cdot 10^{-4}$	$6.66 \cdot 10^{-5}$	$4.08 \cdot 10^{-5}$	$2.63 \cdot 10^{-5}$

N	10^2	10^3	10^4
explicit Euler	$1.1936160 \cdot 10^{-1}$	$1.1449965 \cdot 10^{-2}$	$1.1403143 \cdot 10^{-3}$
backward Euler	$1.1448822 \cdot 10^{-1}$	$1.1398873 \cdot 10^{-2}$	$1.1398000 \cdot 10^{-3}$
RK4	$1.5126559 \cdot 10^{-6}$	$1.4050918 \cdot 10^{-10}$	$1.5951269 \cdot 10^{-14}$

TABLE 3. Error behavior for case (e) $a_8 = 0$, $\rho_0 = 0$, $\rho_{cr} = 4, A_1 = 10, A_2 = 1$ when $A_3 = 5$.

N	$5 \cdot 1$	$5 \cdot 2$	$5 \cdot 3$	$5 \cdot 4$	$5 \cdot 5$
explicit Euler	$3.51 \cdot 10^{-1}$	$3.51 \cdot 10^{-1}$	$2.31 \cdot 10^{-1}$	$1.72 \cdot 10^{-1}$	$1.37 \cdot 10^{-1}$
backward Euler	$3.26 \cdot 10^{-1}$	$3.26 \cdot 10^{-1}$	$2.20 \cdot 10^{-1}$	$1.66 \cdot 10^{-1}$	$1.33 \cdot 10^{-1}$
RK4	$6.86 \cdot 10^{-7}$	$6.86 \cdot 10^{-7}$	$1.33 \cdot 10^{-7}$	$4.15 \cdot 10^{-8}$	$1.69 \cdot 10^{-8}$

N	$5 \cdot 6$	$5 \cdot 7$	$5 \cdot 8$	$5 \cdot 9$	$5 \cdot 10$
explicit Euler	$1.14 \cdot 10^{-1}$	$9.77 \cdot 10^{-2}$	$8.54 \cdot 10^{-2}$	$7.58 \cdot 10^{-2}$	$6.82 \cdot 10^{-2}$
backward Euler	$1.11 \cdot 10^{-1}$	$9.57 \cdot 10^{-2}$	$8.38 \cdot 10^{-2}$	$7.46 \cdot 10^{-2}$	$6.72 \cdot 10^{-2}$
RK4	$8.11 \cdot 10^{-9}$	$4.36 \cdot 10^{-9}$	$2.55 \cdot 10^{-9}$	$1.59 \cdot 10^{-9}$	$1.04 \cdot 10^{-9}$

N	10^2	10^3	10^4
explicit Euler	$3.39659300 \cdot 10^{-2}$	$3.38470334 \cdot 10^{-3}$	$3.38417599 \cdot 10^{-4}$
backward Euler	$3.37172869 \cdot 10^{-2}$	$3.38221709 \cdot 10^{-3}$	$3.38392736 \cdot 10^{-4}$
RK4	$6.47237790 \cdot 10^{-11}$	$7.25560000 \cdot 10^{-15}$	$2.54110000 \cdot 10^{-15}$

In the cases (d)-(e) when ratio $\frac{A_3}{A_2}$ is slightly above 1, some convergence to exact solutions can be observed. However, amplitude of oscillations increases with growing $\frac{A_3}{A_2}$, leading eventually to an unstable solution (see Fig. 3). Nonetheless, for a fixed number of intervals and tending with $N \to \infty$, we still can observe the theoretical convergence rate of both Euler methods and Runge-Kutta scheme (see Table 3).

B. EQUATION (2) WITH REAL WORLD PARAMETERS

In previous section we proved that explicit Euler method (and its modification) gives very satisfactory results for simplified equation (8) and proved stability of this method. This entitles us to perform numerical simulations on more complicated equation (2) with both $\dot{\varepsilon}$ and T time dependent and other parameters (time dependent as well) coming from real world processing of materials. First, let us examine solutions of (8) with parameters established for DP steel and copper through inverse analysis for the experimental data (uniaxial compression tests performed at constant temperatures and strain rates) using algorithm described in [35]. When equation (1) is used to calculate the flow stress, the results which are depicted in Fig. 7, are very similar to those in Fig. 1.

This confirms that indeed, we are ready for modeling of real industrial process. Since it is characterized by strong heterogeneity of deformation, we decided to consider industrial process of hot strip rolling for demonstration of capabilities of the developed model. Similarly to previous laboratory case (see Fig. 7), two materials, DP steel and copper, were considered. Roll pass data, which were the same for both materials, were as follows: initial thickness 20 mm, thickness reduction 50%, roll radius 400 mm and roll rotational velocity 10 rpm. Thermal-mechanical finite element (FE) model was used in the macro scale to calculate strains, stresses and temperatures. Details of the FE code are given in [36] and [37]. Briefly, the

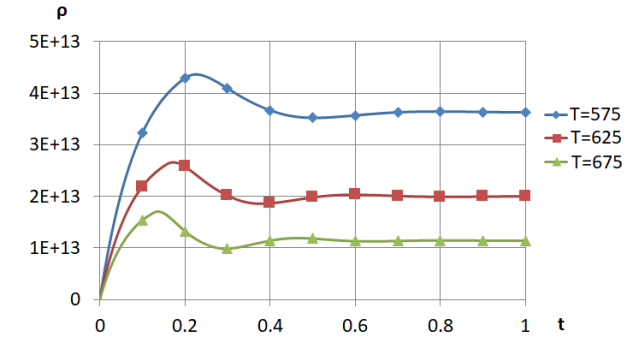

(a) Coefficients for copper in cases:
T=575°C: $A_1 = 5.35882 \cdot 10^{14}, A_2 = 11.134, A_3 = 9.9962 \cdot 10^{-14}$,
T=625°C: $A_1 = 3.91516 \cdot 10^{14}, A_2 = 12.9833, A_3 = 3.30145 \cdot 10^{-13}$,
T=675°C: $A_1 = 2.95672 \cdot 10^{14}, A_2 = 14.8963, A_3 = 9.61261 \cdot 10^{-13}$.

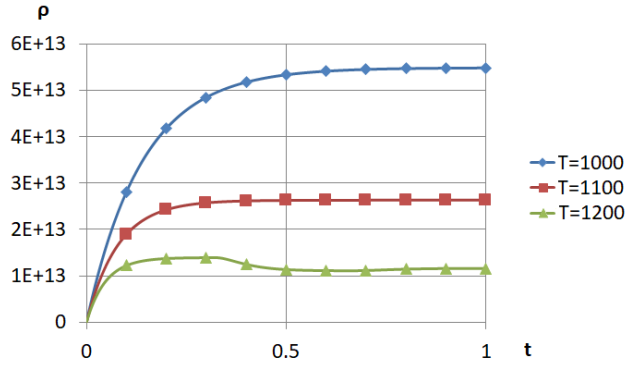

(b) Coefficients for DP steel in cases:
T=1000°C: $A_1 = 3.93394 \cdot 10^{14}, A_2 = 7.17277, A_3 = 6.41439 \cdot 10^{-7}$,
T=1100°C: $A_1 = 3.34986 \cdot 10^{14}, A_2 = 12.7284, A_3 = 1.49657 \cdot 10^{-6}$,
T=1200°C: $A_1 = 2.91544 \cdot 10^{14}, A_2 = 20.895, A_3 = 3.11231 \cdot 10^{-6}$.

FIGURE 7. Calculated solutions for constant temperature T and strain rate $\dot{\varepsilon} = 1$.

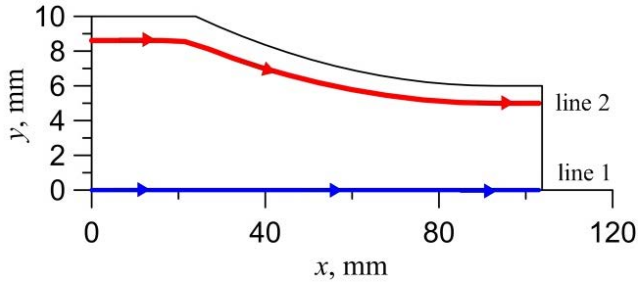

FIGURE 8. Shape of the deformation zone and flow lines along which the model was solved.

Levy-Mises flow rule was used as the constitutive law:

$$\sigma = \frac{2}{3}\frac{\sigma_f}{\dot{\varepsilon}_i}\dot{\varepsilon} \tag{107}$$

where: σ, $\dot{\varepsilon}$ - stress and strain rate tensors, respectively, $\dot{\varepsilon}_i$ - effective strain rate, σ_f - the flow stress provided by (1).

Equation (2) was solved along the flow lines in the deformation zone using current local values of the strain rate and the temperature. The results for two lines, one in the center of the strip and the second one close to the surface (see Fig. 8), are presented on Fig. 11 and 12. Let us explain the details behind these numerical experiments. Due to horizontal symmetry only a top part of the roll gap is shown

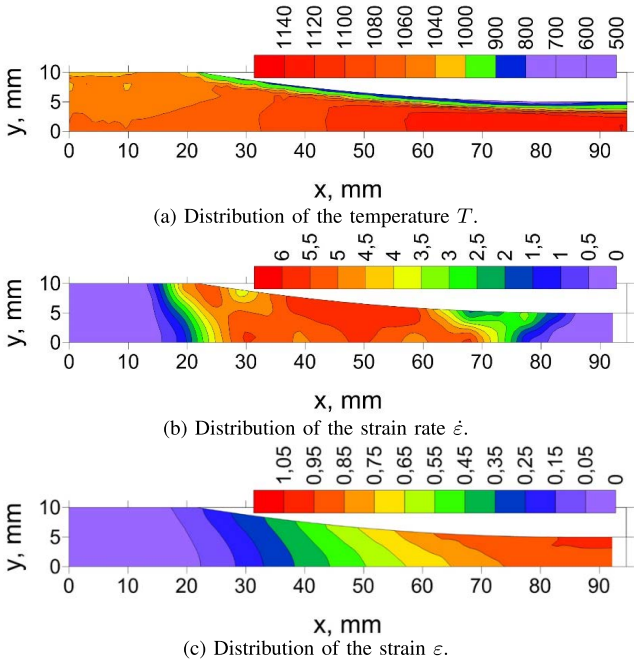

(a) Distribution of the temperature T.

(b) Distribution of the strain rate $\dot{\varepsilon}$.

(c) Distribution of the strain ε.

FIGURE 9. Calculated distribution of the temperature (a), the strain rate (b) and the strain (c) in the roll gap for DP steel.

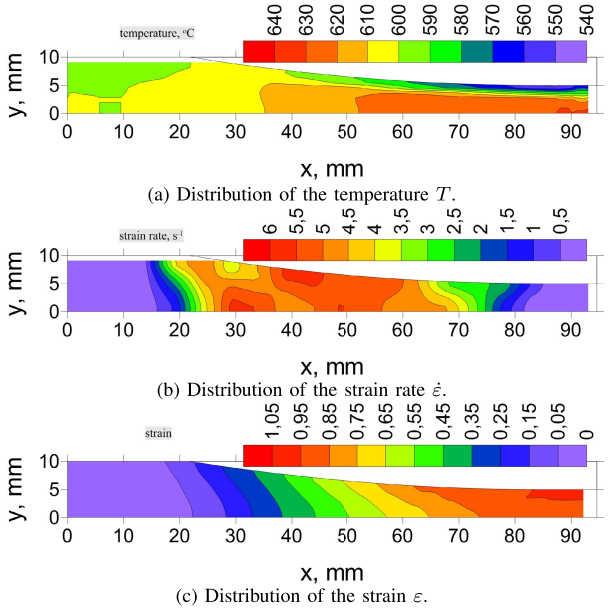

(a) Distribution of the temperature T.

(b) Distribution of the strain rate $\dot{\varepsilon}$.

(c) Distribution of the strain ε.

FIGURE 10. Calculated distribution of the temperature (a), the strain rate (b) and the strain (c) in the roll gap for copper.

in Fig. 8, 9, and 10. The entry temperature was 1060° C for DP steel and 600° C for copper. Shear modulus μ was assumed to be time independent and equal $\mu = 45000$ MPa for copper and $\mu = 75000$ MPa for DP steel. For the assumed parameters the length of the computation domain was 105 mm and the time needed for the material point to flow through this domain was 0.28 s. Finite element (FE) simulation of the rolling process was performed using FE code described in [36] and [37] and calculated distributions of the temperature, strain rate and strain are shown in Fig. 9

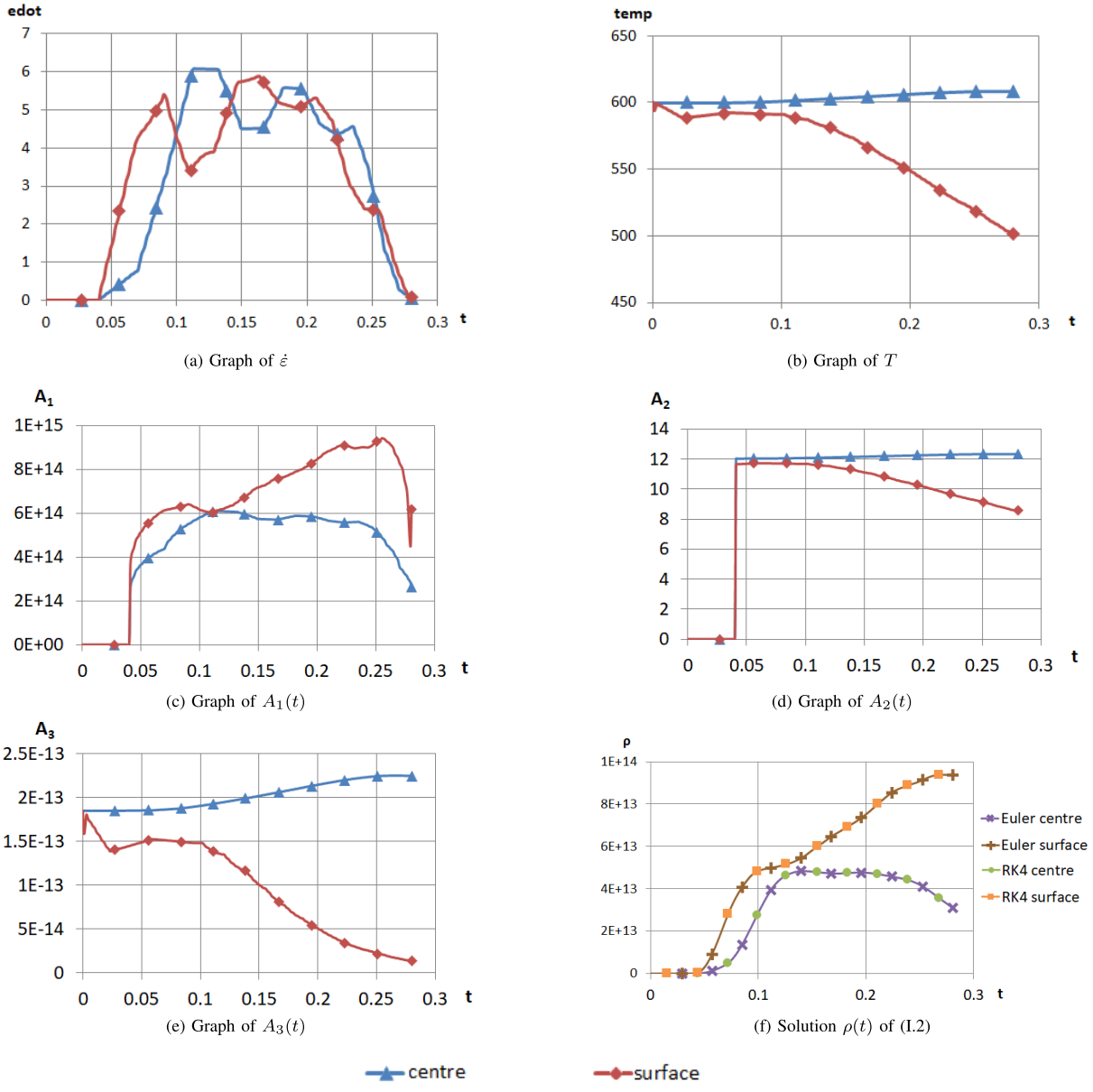

(a) Graph of $\dot{\varepsilon}$

(b) Graph of T

(c) Graph of $A_1(t)$

(d) Graph of $A_2(t)$

(e) Graph of $A_3(t)$

(f) Solution $\rho(t)$ of (I.2)

FIGURE 11. Calculated coefficients and solutions for copper.

and Fig. 10. Results depicted in Fig. 9 are for the DP steel and in Fig. 10 for the copper. On the basis of these results changes of the temperature and the strain rate along the flow lines in Fig. 8 were determined, leading to time-dependent coefficients $A_1(t), A_2(t), A_3(t)$ as presented on Fig. 11 and Fig. 12. Another important coefficient is a_8 as it is responsible for nonlinearity in (2). For copper it was possible to satisfactorily fit the model with $a_8 = 1$, however for DP steel it had to be fractional because $a_8 = 1$ was not leading to satisfactory fitting. Fitting was successful with $a_8 = 0.45239$ and this value was used in our simulations (cf. [36]). By the same reason, the coefficient a_9 was set to 0 for copper and to 0.13751 for DP steel. The coefficient $a_{11} = 10^4$ in both cases, which among other things, ensures that ρ_{cr} is never 0.

We used this data to deal with (2). Calculated evolution solutions ρ with parameters evolving along the lines 1 and 2 in Fig. 8 are presented in Fig. 11 and Fig. 12. Starting density ρ_0 was the same for both metals and equal 10^4 m^{-2}. Analysis of these results shows that they react properly to distinct temperature and strain rate histories for the center and surface areas. Practical observations show that in the center the temperature increases due to deformation heating. Contrary, drop of the temperature due to heat transfer to the cool roll is observed in the surface area. As far as strain rate is considered, in the central part it decreases monotonically due to monotonic deformation of this part. The results presented in Fig. 11 and Fig. 12 replicate properly material behavior in these conditions of the deformation. In the surface area, where

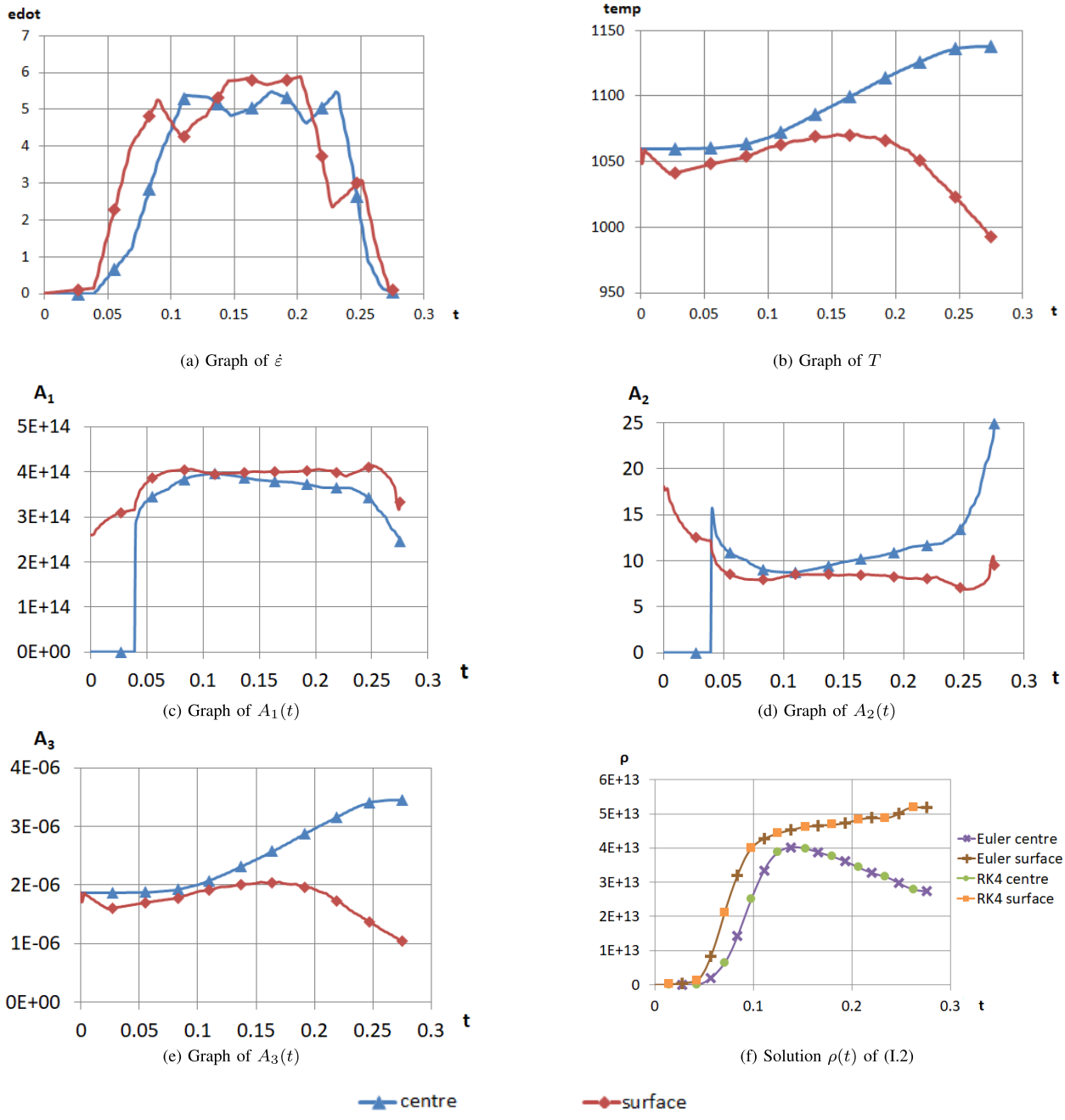

(a) Graph of $\dot{\varepsilon}$

(b) Graph of T

(c) Graph of $A_1(t)$

(d) Graph of $A_2(t)$

(e) Graph of $A_3(t)$

(f) Solution $\rho(t)$ of (I.2)

FIGURE 12. Calculated coefficients and solutions for DP steel.

the temperature is lower and the strain rate is higher, critical dislocation density is higher and so ρ_{cr} given by equation (7) is reached later. In the center of the strip higher temperature leads to more dynamic recrystallization and a decrease of the dislocation density.

Capability to describe microstructure evolution in the varying temperatures and/or strain rates is the main advantage of the model comparing to conventional models, which are phenomenological and predict evolution of the average grain size and resulting flow stress of the material. The conventional models were developed with the objective to reproduce flow stress curves observed in the experiments in constant conditions of deformation. In our approach we account for the effect of recrystallization in an explicit way by considering the history of the evolution of the dislocation density. In consequence, the model describes the phenomenon of the recrystallization accounting for the energy (dislocation density) accumulated in the material and can describe deformation in the varying conditions, which occur in the industrial processes. For constant deformation conditions, our model

predicts flow stress curves which are in agreement with those observed in experiments.

V. CONCLUSION

In the paper we have investigated mathematical aspects of evolution of dislocation density in metallic materials, modeled by delay differential equations (2). For typical range of real world parameters we have shown that the unique solution always exists and it is bounded. For approximation of the solution we have used the explicit Euler method. We have shown the rate of convergence of the Euler method in the case when the right-hand side function is only locally Hölder continuous. We have confirmed our theoretical findings in numerical experiments performed in special cases, when explicit solutions were known. Moreover, we have applied the algorithm to examples with real-world parameters. Despite the fact that for a Runge-Kutta method we have not been able to investigate its error under conditions $(F1)-(F4)$, required by the equation, we tested its numerical behavior taking the Euler scheme as a benchmark. Numerical experiments showed advantage of the Runge-Kutta method over the Euler schemes. This encouraged us to use Runge-Kutta methods in real world applications. Let us emphasize once again, in spite of possible initial believe of triviality in choosing the explicit Euler method to investigate, from theoretical point of view it is highly not obvious that under the nonstandard assumptions it keeps its numerical properties. Therefore, investigation of theoretical properties of the Runge-Kutta method under the assumptions $(F1)-(F4)$ are forwarded to a future work.

REFERENCES

[1] M. Pietrzyk, L. Madej, L. Rauch, and D. Szeliga, *Computational Materials Engineering: Achieving High Accuracy and Efficiency in Metals Processing Simulations*. Amsterdam, The Netherlands: Elsevier, 2015.

[2] J. J. Urcola and C. M. Sellars, "Influence of changing strain rate on microstructure during hot deformation," *Acta Metallurgica*, vol. 35, no. 11, pp. 2649–2657, Nov. 1987.

[3] Y. Estrin and H. Mecking, "A unified phenomenological description of work hardening and creep based on one parameter models," *Acta Metallurgica*, vol. 32, no. 1, pp. 57–70, Jan. 1984.

[4] H. Mecking and U. F. Kocks, "Kinetics of flow and strain-hardening," *Acta Metallurgica*, vol. 29, no. 11, pp. 1865–1875, Nov. 1981.

[5] M. Dikovits, M. C. Poletti, and F. Warchomicka, "Deformation mechanisms in the near-β titanium alloy Ti-55531," *Metall. Mater. Trans. A*, vol. 45, no. 3, pp. 1586–1596, Mar. 2014.

[6] Z. C. Sun, H. Yang, G. J. Han, and X. G. Fan, "A numerical model based on internal-state-variable method for the microstructure evolution during hot-working process of TA15 titanium alloy," *Mater. Sci. Eng., A*, vol. 527, no. 15, pp. 3464–3471, Jun. 2010.

[7] Z. Zhuang, Z. Liu, and Y. Cui, "Dislocation-based single-crystal plasticity model," in *Dislocation Mechanism-Based Crystal Plasticity: Theory and Computation at the Micron and Submicron Scale*. London, U.K.: Academic, 2019, ch. 4, pp. 91–119.

[8] R. H. Buzolin, M. Lasnik, A. Krumphals, and M. C. Poletti, "A dislocation-based model for the microstructure evolution and the flow stress of a Ti5553 alloy," *Int. J. Plasticity*, vol. 136, Jan. 2021, Art. no. 102862.

[9] R. H. Buzolin, M. Lasnik, A. Krumphals, and M. C. Poletti, "Hot deformation and dynamic α-globularization of a Ti-17 alloy: Consistent physical model," *Mater. Des.*, vol. 197, Jan. 2021, Art. no. 109266.

[10] Y. C. Lin, D.-X. Wen, M.-S. Chen, Y.-X. Liu, X.-M. Chen, and X. Ma, "Improved dislocation density-based models for describing hot deformation behaviors of a NI-based superalloy," *J. Mater. Res.*, vol. 31, no. 16, pp. 2415–2429, Aug. 2016.

[11] P. Lisiecka-Graca, K. Bzowski, J. Majta, and K. Muszka, "A dislocation density-based model for the work hardening and softening behaviors upon stress reversal," *Arch. Civil Mech. Eng.*, vol. 21, no. 2, p. 84, May 2021.

[12] P. F. Gao, J. Guo, M. Zhan, Z. N. Lei, and M. W. Fu, "Microstructure and damage based constitutive modelling of hot deformation of titanium alloys," *J. Alloys Compounds*, vol. 831, Aug. 2020, Art. no. 154851.

[13] Y. Q. Ning, X. Luo, H. Q. Liang, H. Z. Guo, J. L. Zhang, and K. Tan, "Competition between dynamic recovery and recrystallization during hot deformation for TC18 titanium alloy," *Mater. Sci. Eng., A*, vol. 635, pp. 77–85, May 2015.

[14] H. J. McQueen, "Development of dynamic recrystallization theory," *Mater. Sci. Eng., A*, vols. 387–389, no. 1, pp. 203–208, Dec. 2004.

[15] K. Huang and R. E. Logé, "A review of dynamic recrystallization phenomena in metallic materials," *Mater. Des.*, vol. 111, pp. 548–574, Dec. 2016.

[16] C. H. J. Davies, "Dynamics of the evolution of dislocation populations," *Scripta Metallurgica et Mater.*, vol. 30, no. 3, pp. 349–353, Feb. 1994.

[17] C. Y. Gao, L. C. Zhang, and H. X. Yan, "A new constitutive model for HCP metals," *Mater. Sci. Eng., A*, vol. 528, nos. 13–14, pp. 4445–4452, May 2011.

[18] S. R. Logan, "The origin and status of the Arrhenius equation," *J. Chem. Educ.*, vol. 59, no. 4, pp. 279–281, 1982.

[19] J. Kitowski, L. Rauch, M. Pietrzyk, A. Perlade, R. Jacolot, V. Diegelmann, M. Neuer, I. Gutierrez, P. Uranga, N. Isasti, G. Larzabal, R. Kuziak, and U. Diekmann, "Virtual strip rolling mill VirtRoll," European Commission Research Programme of the Research Fund for Coal and Steel, TGS, Asker, Norway, Tech. Rep. RFSR-CT-2013-00007, 2017.

[20] C. H. J. Davies, *Private Communication (Data Set Collected From Experiments)*. Clayton, NC, USA: Monash University, 1994.

[21] J. C. Butcher, *Numerical Methods for Ordinary Differential Equations*. 3rd ed. Chichester, U.K.: Wiley, 2016.

[22] E. Hairer, S. P. Nørsett, and G. Wanner, *Solving Ordinary Differential Equations I. Nonstiff Problems*. 2nd ed. New York, NY, USA: Springer-Verlag, 2008.

[23] A. Bellen and M. Zennaro, *Numerical Methods for Delay Differential Equations*. New York, NY, USA: Oxford, 2003.

[24] H. Smith, *An Introduction to Delay Differential Equations With Applications to the Life Sciences* (Texts in Applied Mathematics), vol. 57. New York, NY, USA: Springer, 2011.

[25] W. Cao, J. Liang, and Y. Liu, "On strong convergence of explicit numerical methods for stochastic delay differential equations under non-global Lipschitz conditions," *J. Comput. Appl. Math.*, vol. 382, Jan. 2021, Art. no. 113079.

[26] C. Yue and L. Zhao, "Strong convergence of the split-step backward Euler method for stochastic delay differential equations with a nonlinear diffusion coefficient," *J. Comput. Appl. Math.*, vol. 382, Jan. 2021, Art. no. 113087.

[27] Y. Wang, F. Wu, G. Yin, and C. Zhu, "Stochastic functional differential equations with infinite delay under non-Lipschitz coefficients: Existence and uniqueness, Markov property, ergodicity, and asymptotic log-Harnack inequality," *Stochastic Processes Appl.*, vol. 149, pp. 1–38, Jul. 2022.

[28] Y. Gao and L. Jia, "Stability in mean for uncertain delay differential equations based on new Lipschitz conditions," *Appl. Math. Comput.*, vol. 399, Jun. 2021, Art. no. 126050.

[29] F. Du and J.-G. Lu, "Finite-time stability of neutral fractional order time delay systems with Lipschitz nonlinearities," *Appl. Math. Comput.*, vol. 375, Jun. 2020, Art. no. 125079.

[30] X. Song and J. Peng, "Exponential stability of equilibria of differential equations with time-dependent delay and non-lipschitz nonlinearity," *Nonlinear Anal., Real World Appl.*, vol. 11, no. 5, pp. 3628–3638, Oct. 2010.

[31] P. Morkisz, P. Oprocha, P. Przybyłowicz, N. Z. Czy ewska, J. Kusiak, D. Szeliga, Ł. Rauch, and M. Pietrzyk, "Prediction of distribution of microstructural parameters in metallic materials described by differential equations with recrystallization term," *Int. J. Multiscale Comput. Eng.*, vol. 17, no. 3, pp. 361–371, Jun. 2019.

[32] U. Foryś, M. Bodnar, and J. Poleszczuk, "Negativity of delayed induced oscillations in a simple linear DDE," *Appl. Math. Lett.*, vol. 24, no. 6, pp. 982–986, Jun. 2011.

[33] J. K. Hale, *Ordinary Differential Equations*. 2nd ed. Malabar, FL, USA: Krieger, 1980.

[34] L. Górniewicz and R. S. Ingarden, *Mathematical Analysis for Physicists*. Toruń, Poland: Wydawnictwo Naukowe UMK, 2012.

[35] D. Szeliga, J. Gawad, and M. Pietrzyk, "Inverse analysis for identification of rheological and friction models in metal forming," *Comput. Methods Appl. Mech. Eng.*, vol. 195, nos. 48–49, pp. 6778–6798, Oct. 2006.

[36] J. G. Lenard, M. Pietrzyk, and L. Cser, *Mathematical and Physical Simulation of the Properties of Hot Rolled Products*. Amsterdam, The Netherlands: Elsevier, 1999.
[37] M. Pietrzyk, "Finite element simulation of large plastic deformation," *J. Mater. Process. Technol.*, vol. 106, nos. 1–3, pp. 223–229, Oct. 2000.

NATALIA CZYŻEWSKA received the M.S. degree in mathematics from the AGH University of Science and Technology, Kraków, Poland, in 2019, where she is currently pursuing the Ph.D. degree in mathematics.

Her research interests include numerical analysis for ordinary and delay differential equations, and information-based complexity.

JAN KUSIAK was born in Kraków, Poland, in 1952. He received the M.S. and Ph.D. degrees in control systems (electrical engineering) from the AGH University of Science and Technology, Kraków, Poland, in 1974 and 1978, respectively.

Since 2009, he has been a Full Professor at the AGH University of Science and Technology. He is the author of two books and more than 200 articles in scientific journals. His research interest includes numerical modeling of metallurgical processes, especially on optimization and application of artificial intelligence methods.

PAWEŁ MORKISZ was born in Pszczyna, in 1989. He received the Ph.D. degree in mathematics in 2017.

He was an expert in the fields of numerical methods, stochastic analysis, optimization, and artificial intelligence. He currently works as an Assistant Professor at the Faculty of Applied Mathematics, AGH University of Science and Technology, Kraków. He is also a Mathematician. In addition to his scientific experience, he cooperated with many companies, he has the status of the NVIDIA Deep Learning Institute Ambassador. In business, he is interested in the use of advanced mathematical methods in real problems, including digitalization process for companies and plugging machine learning models into the systems.

PIOTR OPROCHA received the M.S. and Ph.D. degrees in mathematics from Jagiellonian University, Kraków, Poland, in 2002 and 2005, respectively.

Since 2002, he has been employed at the AGH University of Science and Technology, Kraków, where he was promoted to a Full Professor position, in 2018. In 2018, he was awarded the title of a Professor of mathematics by the President of Poland. From 2012 to 2020, he was the Deputy Dean of Science at the AGH University of Science and Technology, and became the Dean, in 2020. His research interests include dynamical systems, ergodic theory, optimization, and applications of mathematics in engineering problems.

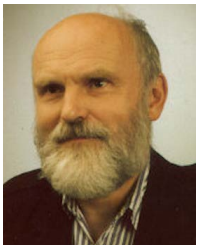

MACIEJ PIETRZYK was born in Kraków, Poland, in 1947. He received the M.S. degree in electrical engineering and the Ph.D. degree in materials engineering from the AGH University of Science and Technology, Kraków, in 1970 and 1975, respectively.

In 1992, he became a Full Professor at the AGH University of Science and Technology. He is the author of four books and more than 500 articles in scientific journals. His research interests include numerical modeling of metal forming processes and phase transformations during heat treatment. Particular emphasis in his research is on the development of material models and on application of the inverse analysis to identification of these models.

PAWEŁ PRZYBYŁOWICZ was born in Tarnów, Poland, in 1983. He received the M.S. and Ph.D. degrees in mathematics from the AGH University of Science and Technology, in 2007 and 2011, respectively, and the Habilitation degree in mathematics, in 2019.

He currently works at the Faculty of Applied Mathematics, AGH University of Science and Technology. He is the author or coauthor of more than 30 articles. He works in the field of numerical analysis for ordinary and stochastic differential equations, information-based complexity, and Monte Carlo simulations on GPUs. He is an Associate Editor of *Journal of Complexity* and *Opuscula Mathematica*.

Dr. Przybyłowicz was a recipient of the Information-Based Complexity Young Researcher Award in 2012, the DAAD Scholarship in 2013, and the Joseph Traub Information-Based Complexity Award in 2018.

ŁUKASZ RAUCH was born in Bielsko-Biała, in 1978. He received the first M.Sc. degree in computer science and the second M.Sc. degree in management and marketing from the AGH University of Science and Technology, in 2002 and 2003, respectively, and the Ph.D. degree, in 2006. He defended his Ph.D. thesis in computer science.

From 2016 to 2020, he was the Head of the Department of Applied Computer Science and Modelling, AGH University of Science and Technology. Since 2020, he has been the Deputy Dean for science and cooperation at the Faculty of Metals Engineering and Industrial Computer Science, AGH University of Science and Technology. He shares his scientific interests between computer science and its applications in modeling and design of industrial processes. He is the author of more than 200 scientific papers published in international and national journals, and presented during conferences or workshops. He participated in many scientific and research and development projects realized in cooperation with large companies as well as with SMEs. This work he holds in the highest regard since the scientific solutions find a practical application in industry.

DANUTA SZELIGA was born in Strzelce Opolskie, Poland, in 1971. She received the M.Sc. degree in computer science from Jagiellonian University, Kraków, Poland, in 1996, and the Ph.D. (Hons.) and Habilitation degrees in material engineering (applied computer science) from the AGH University of Science and Technology, Kraków, in 2001 and 2014, respectively.

Since 2019, she has been the Head of the Department of Applied Computer Science and Modelling, Faculty of Metals Engineering and Industrial Computer Science, AGH University of Science and Technology. She is the coauthor of three books and more than 140 articles in scientific journals. Her research interests include numerical modeling of forming processes, applications of inverse method, sensitivity analysis for identification of parameters of materials and numerical models, and optimization of manufacturing material science processes.